Advanced Semiconductor and Organic Nano-Techniques (Part II)
H. Morkoç (Ed.)

CHAPTER 6

Single-Walled Carbon Nanotubes for Nanoelectronics

M. S. Fuhrer

UNIVERSITY OF MARYLAND, COLLEGE PARK, MARYLAND

I. Introduction

Around 1991, inspired by the discovery and mass production of cage-like fullerene molecules, several research groups began to consider the properties of a hypothetical carbon structure: a single layer of graphite wrapped into a seamless cylinder—the carbon nanotube (Hamada *et al.* 1992; Mintmire

et al. 1992; Saito *et al*. 1992a). It was soon realized that carbon nanotubes may be metallic or semiconducting, and should be excellent one-dimensional (1D) conductors at room temperature. About the same time, carbon deposits resulting from the arcing of graphite rods to obtain fullerenes were investigated via transmission electron microscope (TEM) and revealed to contain concentrically nested carbon nanotubes (Iijima 1991) ("multi-walled carbon nanotubes" or MWNTs). Soon thereafter, single-walled carbon nanotubes (SWNTs) were synthesized (Bethune *et al*. 1993; Iijima and Ichihashi 1993). Measurments soon revealed a material with an extraordinary convergence of exceptional thermal, mechanical, and electrical properties: the thermal conductivity of individual MWNTs exceeds that of diamond at room temperature (Kim *et al*. 2001); the elastic modulus of carbon nanotubes may exceed 1 TPa, making them the strongest known fibers (Treacy *et al*. 1996; Wong *et al*. 1997; Poncharal *et al*. 1999); electrons are transported ballistically through SWNTs over distances greater than 1 μm at room temperature (Bachtold *et al*. 2000).

The first electrical experiments on individual metallic SWNTs were reported in 1997 (Bockrath *et al*. 1997; Tans *et al*. 1997), with experiments on individual semiconducting SWNTs in 1998 (Tans *et al*. 1998b). In the following 5 years, research into the electrical properties of nanotube devices has exploded. A picture has emerged of a material with superlative electrical properties: metallic SWNTs have conductivities comparable to the best metals, and can carry current densities exceeding 10^9 A/cm^2; semiconducting SWNTs have mobilities exceeding the best silicon MOSFETs. Still, enormous challenges remain to incorporating this material into a useful device technology: nanotubes are still expensive to manufacture, currently nanotubes cannot be sorted according to electronic property (metallic and semiconducting nanotubes are randomly mixed), and methods for placing nanotubes with precision onto substrates are in their infancy.

This chapter will serve to review the current status of research on carbon nanotubes for nanoelectronics applications. The focus will be on single-walled carbon nanotubes, whose properties are closest to ideal, though some of the conclusions will also apply to multi-walled nanotubes. It should be noted that there exist a number of excellent reviews of the electronic transport properties of individual single-walled (Dekker 1999; Nygard *et al*. 1999; McEuen 2000; Louie 2001; Yao *et al*. 2001) and multi-walled carbon nanotubes (Schonenberger *et al*. 1999; Schonenberger and Forró 2000; Forró and Schonenberger 2001).

This chapter is structured as follows. Sections II–IV will serve as a review of the fundamental theoretical and experimental work on the electronic properties of carbon nanotubes. Section II will introduce the theory of the electronic structure of carbon nanotubes, including the remarkable dependence of their electronic properties on structure. Section III will discuss the synthesis of carbon nanotubes, as well as the techniques used to place

individual nanotubes into electronic circuits. Section IV will discuss the room temperature and cryogenic electronic transport properties of individual metallic and semiconducting SWNTs.

Section V will give an overview of the current state of research on nanoscale electronic devices incorporating carbon nanotubes. These devices range from field-effect and single-electron transistors to more exotic junction devices and electromechanical devices. Some significant advantages of carbon nanotubes for nanoelectronics become obvious: the exposed channel of the semiconducting nanotube transistor makes it an excellent candidate for chemical and biological sensing, the geometry of the carbon nanotube automatically guarantees small junction capacitance and high transconductance in nanotube single-electron transistors, the long electron mean free paths and high thermal conductivity in nanotubes suggests their use as interconnects to devices located at nanotube junctions, and the high stiffness and robustness of nanotubes makes them attractive for high-speed mechanical devices.

Sections VI–VII will attempt to look to the future of nanotube research. Section VI discusses the challenges that stand in the way of developing nanotube devices into useful technologies, such as the production of electronically uniform material, and the development of techniques for precise placement of nanotubes within circuits. Section VII will move beyond carbon nanotubes to pose the question: Are there other materials that have some of the advantageous properties of carbon nanotubes, but avoid some of the difficulties? Indeed a rapidly growing number of non-carbon nanotubes and nanowires have been synthesized, some with very attractive properties.

II. Electronic Properties of Carbon Nanotubes

Soon after the discovery of fullerene synthesis by the arc-discharge technique, it was found that, after arcing, the carbon cathode held a deposit which was dense in nanotubes (Iijima 1991). TEM imaging of these tubules showed that they consisted of concentric shells of seamless graphene sheets. These carbon nanotubes were found to have between two and over 50 walls, and be many micrometers in length. It was later found that the presence of certain transition metals in the arc catalyzed the production of carbon nanotubes with only one layer (Bethune *et al.* 1993; Iijima and Ichihashi 1993). This divided nanotubes into two classes: single-SWNTs and MWNTs.

Even before the discovery of carbon nanotubes by Iijima (1991), several research groups became interested in the possibility of extending the fullerene cage structure into a one-dimensional wire. Soon after the publication of Iijima's discovery, three groups published results on the electronic structure of SWNTs (Hamada *et al.* 1992; Mintmire *et al.* 1992; Saito *et al.* 1992a). It was realized that this new form of carbon could be metallic or

semiconducting depending sensitively on its atomic structure (Hamada *et al.* 1992; Saito *et al.* 1992a,b), and that the Peierls distortion, to which all 1D metals are unstable, should occur only at very low temperatures in metallic nanotubes (Mintmire *et al.* 1992).

1. BAND STRUCTURE OF CARBON NANOTUBES

Graphite is the starting point for considering the electronic structure of the carbon nanotube. Graphite is a solid form of carbon in which the atoms are covalently bonded in a hexagonal network to form 2D planes, called graphene, with the planes weakly bonded together through the van der Waals interaction. Figure 1(a) shows the graphene atomic structure. The low-energy band structure of graphene is unusual [see Fig. 1(b)]; the bands are cones, meeting in points at the Fermi surface at the K points in the Brillouin zone. In most directions in k-space, graphene is a semiconductor, only for special directions [e.g., k_y, in Fig. 1(b)] is graphene metallic.

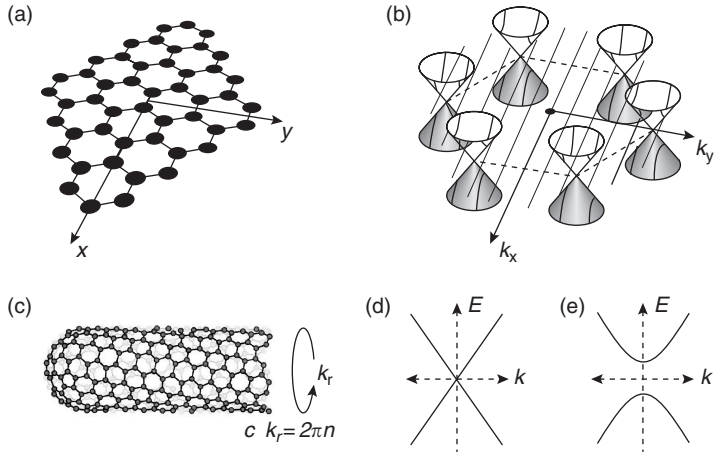

FIG. 1. Band structure of the single-walled carbon nanotube. The atomic structure of the graphene sheet is shown in (a). The band structure for low-energy excitations is shown schematically in (b), with k_x and k_y the wavevectors in the x and y directions in (a). The bands are cones, which meet the Fermi surface at points located at the corners of the hexagonal Brillouin zone (shown by the solid hexagon). When the graphene sheet is rolled up to form a nanotube (c), the circumferential wavevector k_r is quantized, such that $c \cdot k_r = 2\pi n$, where c is the circumference and n is an integer. The 1D bands are slices of the 2D band structure in (b) taken at the allowed values of k_r. The thin lines in B show the slices for a particular semiconducting SWNT. D and E show the resulting 1D band structures at low energies for the metallic and semiconducting nanotubes respectively. The metallic nanotube (d) has two linear bands which cross at the Fermi level. The semiconducting nanotube (e) has two hyperbolic bands, with an energy gap $E_g \approx 600\,\text{meV}$ for a 1.5-nm diameter nanotube.

Conceptually, an SWNT may be formed by cutting a strip of the graphene sheet and rolling it into a tube (Saito *et al.* 1992b). The lattice vector on the graphene sheet that connects the two points that will roll into each other is called the circumferential vector $\boldsymbol{c}$, and completely defines the type of SWNT. SWNTs are then denoted by their circumferential vector in terms of the graphene lattice vectors $\boldsymbol{a}_1$ and $\boldsymbol{a}_2$; thus, an SWNT with a circumferential vector $n_1\boldsymbol{a}_1 + n_2\boldsymbol{a}_2$ would be denoted (n_1, n_2). (Two non-chiral types of tubes exist and are given special names in the literature: (n, n) tubes are called armchair and $(n, 0)$ tubes are called zig-zag, after the shapes of the bands of carbon atoms which encircle each nanotube.)

The electronic structure of an SWNT may be approximated by simply taking the electronic structure of the graphene sheet and quantizing it in the circumferential direction such that $\boldsymbol{c} \cdot \boldsymbol{k}_r = 2\pi n$, where n is an integer (Saito *et al.* 1992b). [Other calculations give similar results (Hamada *et al.* 1992; Mintmire *et al.* 1992).] This condition is equivalent to stating that the electronic wavefunction on the tube be single-valued around the circumference. Thus the graphene sheet is sliced at regular intervals in k-space [see Fig. 1(b)]. The result is a 1D dispersion relation with many sub-bands corresponding to the various slices.

The bands of the graphene sheet only cross the Fermi surface at the K point. This means only those tubes whose band structure slices cross the K point will be metallic. For a tube (n_1, n_2) this can be expressed by the condition: $n_1 - n_2 = 3q$ where q is an integer. A more careful treatment (Hamada *et al.* 1992) which takes into account the curvature of the graphene sheet finds that only the tubes with $n_1 = n_2$ will be metallic, the other tubes satisfying $n_1 - n_2 = 3q$, with non-zero q will have a small gap on the order of milli electron-Volts, considerably smaller than room temperature.

The low-energy band structure of metallic and semiconducting SWNTs is depicted in Fig. 1(d) and (e). Metallic SWNTs have two linear bands which cross at the Fermi level. Semiconducting SWNTs have two hyperbolic bands, separated by an energy gap, with $E_g \approx 900\,\text{meV}/d$, where d is the diameter in nanometers. In both cases, the next closest bands are on order 500 meV away for typical diameter SWNTs; thus SWNTs are extremely 1D at room temperature, where the thermal energy is 25 meV.

This result is quite striking. It is an extreme example of a size effect in small structures, and manifests because of the unusual nature of the graphene Fermi surface—metallic for some directions in k-space, and semiconducting in others. This result has been verified by simultaneous measurement of the geometry and electronic structure of individual SWNTs by scanning tunneling microscope (STM) (Odom *et al.* 1998; Wildoer *et al.* 1998). In these experiments, the atomic structure of individual SWNTs was measured topographically by the STM, and then the STM tip was placed at a fixed distance above the SWNT to perform tunneling spectroscopy measurements

of the band structure. The results were in excellent agreement with the model presented above.

The large number of possible band structures for SWNTs would seem to speak against their possible usefulness as an electronic material, unless the atomic structure of nanotubes could be controlled exactly. However, the picture is less complicated than is immediately obvious. It was soon pointed out that SWNTs fall into three broad classes: metallic SWNTs with $n_1 = n_2$, small-gap semiconducting SWNTs with $n_1 - n_2 = 3q$ but $q \leq 0$, and moderate-gap semiconducting SWNTs, with $n_1 - n_2 \leq 3q$. Furthermore, the typical energy gaps of the semiconducting SWNTs were found to depend almost entirely on diameter d, with the moderate semiconducting gaps scaling as $1/d$ and the small semiconducting gaps scaling as $1/d^2$ (Kane and Mele 1997). In fact, all the features in the density of states are determined to good approximation by diameter alone (Mintmire and White 1998). Since the energy gaps in small-gap semiconducting SWNTs are smaller than room temperature for $d > 1.4\,\text{nm}$ (Kane and Mele 1997), these SWNTs may be grouped with the metallic SWNTs for the purposes of room temperature applications. SWNTs may be produced with narrow diameter distributions, so the problem of obtaining an electronically uniform material is reduced to the separation of SWNTs into two classes, metallic (including small band-gap semiconductor) and large-gap semiconductor. More will be said on this issue below in Section VI.

2. PEIERLS DISTORTION

All 1D metals are unstable to a Peierls distortion, a periodic modulation of the atomic positions which opens a gap at the Fermi surface (Peierls 1955). For instance, in polyacetylene, a 1D chain of carbon atoms, the symmetry of the chain is broken by alternating single and double bonds. The Peierls transition temperature T_c, above which the system would be metallic, is given by $k_B T_c \approx 0.28\, E_g$, where k_B is Boltzmann's constant, and E_g is the Peierls energy gap. For polyacetylene, the Peierls energy gap is $\sim$1.4 eV (Su *et al.* 1980) therefore T_c is $\sim$5000 K, significantly greater than room temperature, and in fact significantly greater than the decomposition temperature of the polymer.

Mintmire, Dunlap and White estimated the Peierls temperature for a (5,5) metallic SWNT to be of order 1 K, orders of magnitude below that of polyacetylene. The reason for the much lower Peierls transition temperature in SWNT is a much smaller gain in electronic energy *per carbon atom*, since the one dimensional state is shared over, for example, 10 carbon atoms around the circumference of the (5,5) SWNT, compared with a slightly greater (1.5×) elastic energy cost per carbon atom to distort the carbon–carbon

bonds in the three-fold-coordinated SWNT lattice compared to the two-fold-coordinated polyacetylene.

More careful analyses of the particular phonon modes and electron–phonon coupling involved in Peierls distortion of a metallic SWNT lead to estimates of the Peierls transition temperature as below 9 K (Huang *et al.* 1996) and 15 K (Sedeki *et al.* 2000), still well below room temperature.

3. SUMMARY OF ELECTRONIC STRUCTURE

SWNTs may be metallic or semiconducting, depending very sensitively on how the graphene sheet is wrapped up to form the nanotube. However, the gross features in the density of states are determined by diameter alone, so nanotubes of a given diameter fall into three classes: metallic, small band-gap semiconductor, and moderate band-gap semiconductor. For room temperature purposes, small band-gap semiconductor SWNTs may be treated as metallic. For example, SWNTs of diameter 1.5 nm will be either metallic, or semiconducting with a bangap $E_g \approx 0.6\,\text{eV}$. Nanotubes are highly 1D: a 1.5-nm SWNT has a sub-band spacing of order 1 eV, much greater than the room temperature thermal energy of 25 meV.

Because of the high stiffness and small number of 1D modes of the nanotube (low density of states) nanotubes are relatively immune to the Peierls distortion, which destroys metallicity. The Peierls transition is estimated to occur only well below room temperature in metallic SWNTs.

III. Nanotube Synthesis and Device Fabrication

1. SYNTHESIS OF SINGLE-WALLED CARBON NANOTUBES

It is now known that SWNTs may be synthesized by a variety of methods. These methods have in common a source of carbon and a catalyst, typically a transition metal, such as iron, nickel, cobalt, yttrium, or molybdenum, in the form of nanoparticles. The basic picture that arises is that of a vapor–liquid–solid reaction; atomic carbon dissolves in a small metal particle, and, once supersaturated, the particle extrudes solid carbon. A graphite tube satisfies the need to extrude a narrow carbon shape with no dangling bonds.

The first SWNTs were synthesized in a carbon plasma obtained by striking an electric arc between carbon rods containing small amounts of catalyst, typically iron, nickel, cobalt, and/or yttrium (Bethune *et al.* 1993; Iijima and Ichihashi 1993; Journet *et al.* 1997). Higher yields were demonstrated by vaporizing a similar carbon target with intense laser pulses (Thess *et al.* 1996).

In both cases, the plasma is surrounded by an inert atmosphere, such as helium. Unlike MWNTs, which form as a growth on the cathode during arc synthesis (without a catalyst), SWNTs deposit on the synthesis chamber walls.

SWNTs synthesized by these methods are found by TEM to form bundles of tens or hundreds of nanotubes arranged in a triangular lattice. Along with the nanotube bundles, fullerenes, amorphous carbon, and metal catalyst particles are also seen in the as-formed material.

Several techniques have been employed to purify the as-grown SWNT material. Baking in a vacuum oven at 1000°C removes much of the metal catalyst and fullerenes. Alternatively, soluble fullerenes may be removed with toluene or CS_2, and the insoluble material may be suspended in surfactant-containing H_2O via ultrasonication and then filtered (Bandow *et al.* 1997; Rao *et al.* 1997). Refluxing in boiling nitric acid before washing and filtration has been found to be effective at removing the catalyst particles and amorphous carbon (Rinzler *et al.* 1998).

Various methods have been derived to separate nanotubes from bundles in suspension or solution. Ultrasonication of SWNT material that has been purified by baking in a vacuum oven in dichloroethane (DCE) results in a suspension of small bundles and some individual SWNTs. More recent efforts to solubilize nanotubes will be discussed in Section VI.

Chemical vapor deposition (CVD) offers an alternative synthesis method. SWNTs have been prepared via CVD from a carbon-containing feedstock gas, such as carbon monoxide (Dai *et al.* 1996), methane (Kong *et al.* 1998), or ethylene (Hafner *et al.* 1998). In general, a nanostructured transition metal catalyst is prepared, and the carbon feedstock gas is flowed over the catalyst at high temperature. The catalyst catalyzes the decomposition of the feedstock gas, and carbon dissolves in the catalyst particles. Once supersaturated, the catalyst particles extrude excess carbon in the form of nanotubes.

The CVD synthesis technique has been used to successfully prepare carbon nanotubes directly on flat substrates which are suitable for electronic device fabrication (Kong *et al.* 1998; Hafner *et al.* 2001). Kong *et al.* (1998) used a catalyst of alumina nanoparticles coated with iron and molybdenum. This catalyst could be patterned into islands on a flat SiO_2-capped silicon wafer substrate using a conventional lift-off lithography technique. The substrate supporting the catalyst was exposed to flowing methane at 900°C. After CVD, SWNTs were found lying on the flat substrate anchored to the catalyst islands. Hafner *et al.* (2001) prepared a catalyst of iron nanoparticles by depositing a thin film of ferric nitrate deposited on the substrate simply by dipping the substrate into a ferric nitrate solution in 2-propanol followed by rinsing in hexane. The ferric nitrate was reduced to iron in a hot hydrogen-containing atmosphere, followed by CVD growth using ethylene as the feedstock gas at 700°C. This method produced SWNTs dispersed about the surface of the substrate. Some of the SWNTs were found to be projecting

upward from the substrate after growth, and could be plucked from the surface by a passing atomic force microscope (AFM) tip. Unlike the arc- and laser-ablation derived SWNT material, most CVD-grown SWNTs are found as individual nanotubes, with a few small bundles are formed. However, the size distribution of CVD-grown SWNTs is typically much larger.

2. FABRICATION OF ELECTRONIC DEVICES

The first attempts to attach electrodes to individual SWNTs were made using material derived from the laser ablation process (Bockrath *et al*. 1997; Tans *et al*. 1997). These SWNTs were suspended in DCE via ultrasonication and then deposited on SiO_2-capped silicon substrates by spinning or simply applying a drop of suspension to the substrate for a short time and then washing off the excess solution with 2-propanol.

Two schemes for contacting SWNTs with electrodes were initially investigated: deposition of SWNTs on top of prepatterned electrodes ("tube-on-top") and evaporating metal electrodes on top of SWNTs after deposition ("metal-on-top"). Figure 2 shows AFM images of examples of each top of device, and illustrates each schematically. The prototypical SWNT device has two electrodes attached to the SWNT ("source" and "drain") and a third "gate" electrode (either the conducting silicon substrate beneath the oxide, or a nearby metallic electrode).

Tube-on-top devices were fabricated by prepatterning gold or platinum electrodes and then depositing SWNTs from suspension by spin coating or

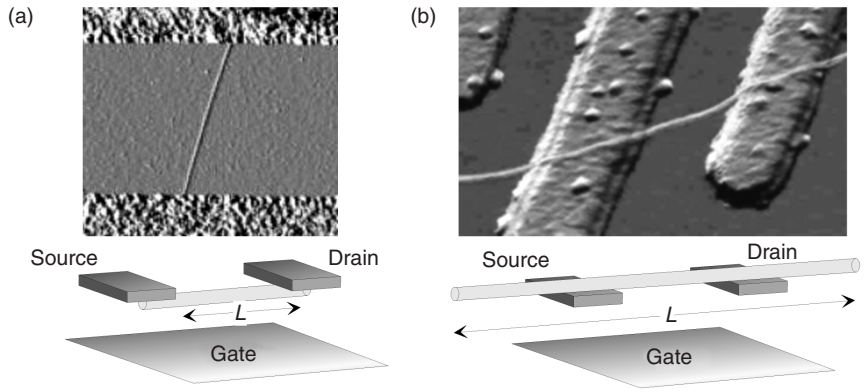

FIG. 2. An AFM image of a "metal-on-top" device is shown in (a). The rough areas at top and bottom are Cr/Au electrodes, and the narrow line is the nanotube, lying on an SiO_2-capped Si substrate. A schematic of the device is shown below. A "tube-on-top" device is shown in (b) (image courtesy Cees Dekker). Here, a nanotube (thin line) was deposited from solution over pre-patterned Pt leads on SiO_2-capped Si. The metal leads are spaced approximately 140 nm apart. The lower panel shows a schematic of the device.

immersion in solution followed by rinsing. In general, tube-on-top devices were found to have higher contact resistances than metal-on-top devices. It was speculated that this was due to the sharp bending of the nanotube over the contacts (Bezryadin *et al*. 1998), which could open an electronic energy gap in a nominally metallic SWNT. This theory was born out by the fact that the contact resistance of tube-on-top devices was improved by planarizing the contacts before deposition (Yao *et al*. 2000).

Metal-on-top devices were fabricated by first depositing SWNTs on substrates, and then patterning electrodes via a liftoff process. Bockrath *et al*. (1997) developed a technique to contact specific individual SWNT that had been located with AFM. First a pattern of metal (Cr/Au) alignment marks was defined on the substrate using conventional electron-beam lithography and lift-off. An AFM was then used to image the SWNTs relative to the alignment marks. Resist was again spun on the substrate, and a second electron-beam lithography step established electrical contacts to the desired nanotubes.

Kong *et al*. (1998) exploited the ability to pattern the catalyst for CVD growth of SWNTs to fabricate devices with high yield. Islands of catalyst were patterned on substrates with separations of a few micrometers using electron beam lithography and lift-off. After CVD growth of SWNTs, a second lithography step was used to cover the areas containing the catalyst islands with metal electrodes. Often SWNTs would span the gaps between catalyst islands, and would thus be contact by the electrodes.

IV. Electronic Transport Properties

In general, the device behavior of individual two-terminal SWNT devices was found to fall into two classes. One class, identified as metallic, has a source–drain conductance that is nearly independent of voltage applied to the gate electrode (see Fig. 3). The other class, identified as semiconducting, has a source–drain conductance that depends strongly on gate voltage V_g, conducting at negative V_g, and becoming insulating at positive V_g (see Fig. 3). This behavior is reminiscent of a p-type field-effect transistor (FET), and hence the semiconducting SWNT device has been termed the tube-FET or NT-FET. More will be said below in Section V.1 about the theory of operation of the semiconducting SWNT FET.

1. Conductance Quantization in One Dimension

The starting point for the discussion of electronic transport properties of highly 1D SWNTs is the Landauer conductance formalism. Landauer (1958)

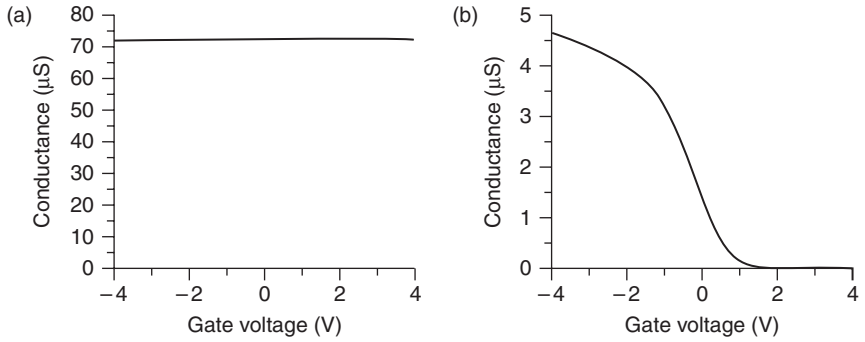

FIG. 3. The conductance G as a function of gate voltage V_g for metallic and semiconducting SWNT devices at room temperature. The conductance of the metallic nanotube (a) is nearly independent of gate voltage, while the conductance of the semiconductaing nanotube (b) varies strongly with gate voltage, conducting at negative gate voltage, and becoming insulating at positive gate voltage. Both devices are "metal-on-top", fabricated using nanotubes prepared by CVD.

first derived the conductance of an ideal (zero scattering, or ballistic) 1D channel, and found the surprising result that the conductance was finite, and quantized: the conductance $G = e^2/h$ for each mode of the channel, where e is the electronic charge, and h is Planck's constant [for a general discussion, see, e.g., Datta (1995)]. The general result for a 1D channel with multiple modes and less than unity transmission probability is

$$G = \frac{e^2}{h} \sum_i T_i$$

where T_i is the transmission probability of the ith mode. For an individual metallic SWNT, there are two doubly-spin-degenerate bands at the Fermi level, and the conductance in the absence of scattering would be $4e^2/h$, or approximately 155 μS (the result would be the same for a semiconducting nanotube, as long as the Fermi level lies with in the first sub-band, due to electrostatic or chemical doping). This corresponds to a minimum resistance of approximately 6.5 kΩ for a single SWNT. This quantized resistance appears as a contact resistance—a drop in the electrochemical potential occurs at each contact to the SWNT.

Using the Landauer formalism in the ohmic (classical transmission) limit (the phase relaxation length is less than the distance between scatterers), the two-terminal resistance of a nanotube device is

$$R = h/4e^2 + R_\mathrm{i} + R_\mathrm{c1} + R_\mathrm{c2}$$

where $h/4e^2$ is the quantized contact resistance of the nanotube, R_i the intrinsic resistance from scattering processes within the tube arising from,

for example, disorder or phonons, and the contact resistances $R_{c1,2}$ the resistances due to transport barriers formed at the metal electrode/nanotube junctions.

2. METALLIC SINGLE-WALLED NANOTUBES

a. Two-Terminal Conductance at Room Temperature

The first metallic SWNT devices fabricated and measured in 1997 had two-terminal resistances ranging from tens of kilo ohms to mega ohms (Bockrath *et al*. 1997; Tans *et al*. 1997) significantly greater than the minimum resistance of $\sim 6.5\,\mathrm{k}\Omega$. It is difficult to separate the contact resistances $R_{c1,2}$ from the intrinsic resistance R_i in mesoscopic devices. In macroscopic devices, a four-terminal measurement may be made, but the placement of additional strongly interacting voltage probes onto a SWNT will significantly disturb the measurement. Electrostatic force microscopy (EFM) provides a way around this dilemma (Bachtold *et al*. 2000). In an EFM measurement, a conducting-tip AFM probe is used as a local voltmeter which interacts only weakly with the device under test.

Figure 4 shows an EFM measurement of the voltage in a current-carrying metallic SWNT device (Bachtold *et al*. 2000). The two-probe resistance of this 2.5 nm diameter bundle is 40 kΩ. (From the current-carrying capacity of the bundle, it was estimated that two metallic SWNTs were present.) The EFM image of this SWNT bundle, as well as a line trace along the backbone of the bundle is shown in the figure. The potential is flat over its length,

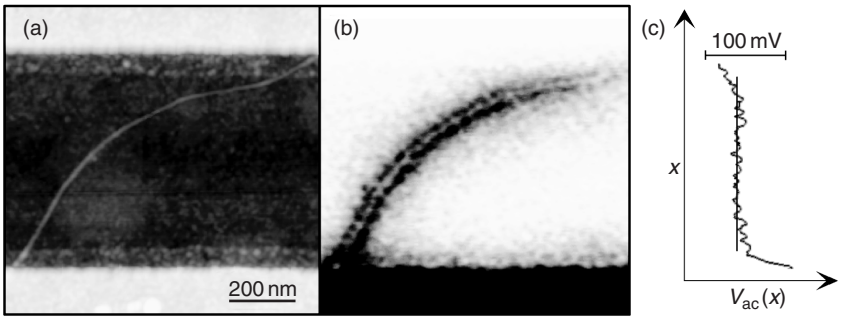

FIG. 4. EFM measurement of a metallic SWNT bundle at room temperature (Bachtold *et al*. 2000). A topographic AFM image is shown in (a); the white areas at top and bottom are the Cr/Au electrodes, and the faint white line is the nanotube. The EFM signal is shown in (b); 100 mV was applied to the bottom electrode, and the top electrode was grounded. The total device resistance is 40 kΩ. A trace of the local voltage along the backbone of the nanotube is shown in (c). The voltage drops at each contact, but is flat in between ($R < 3\,\mathrm{k}\Omega$), indicating ballistic conduction over the length of the nanotube (~1.6 μm).

indicating no measurable intrinsic resistance; R_i of the bundle was estimated to be at most 3 kΩ. The contact resistances are measured to be approximately 28 and 12 kΩ for the upper and lower contacts, respectively.

The measured resistance may be related to a transmission probability using the four-terminal Landauer formula: $R_i = (h/4e^2)(1 - T_i)/T_i$ per nanotube, where T_i is the transmission coefficient for electrons along the length of the nanotube. Here $T_i > \frac{1}{2}$: the majority of electrons traverse the bundle without scattering. Transport in metallic nanotubes is ballistic over a length of >1 μm, even at room temperature. This result indicates that the resistance of metallic SWNT devices arises from imperfect contact resistances and not from intrinsic scattering within the nanotube.

A number of techniques have been employed to improve the contact resistance of SWNT devices. The best contacts have been obtained by evaporating Au or Pt over the tube, often followed by a subsequent anneal. A number of groups have seen conductances approaching the value $G = 4e^2/h$ (Kong *et al.* 2001; Liang *et al.* 2001). Figure 5 shows the differential conductance dI/dV as a function of V_{sd} for a 1 μm long SWNT with low contact resistance. At low V_{sd}, the conductance is $\sim 2\,e^2/h$ at room temperature, growing to $\sim 3.3\,e^2/h$ as the temperature is lowered, implying an intrinsic resistance $R_i < 3.3$ kΩ at room temperature, and <1.4 kΩ at low temperature. For a 1.5 nm diameter tube, this corresponds to a room temperature resistivity ρ less than 10^{-6} Ω cm. The conductivity of metallic nanotubes at room temperature can thus be equal to, or even exceed, the conductivity of the best metals at room temperature.

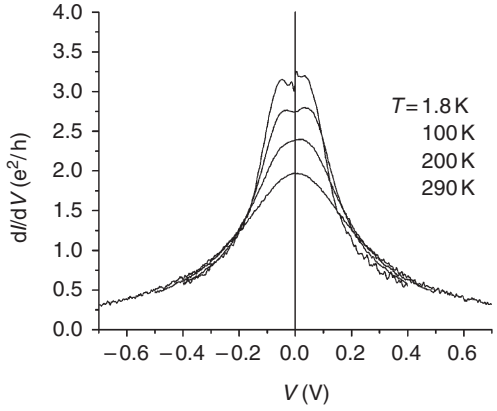

FIG. 5. Differential conductance as a function of bias voltage for a metallic SWNT device at temperatures 1.8, 100, 200, and 290 K. At zero bias, the conductance rises as the temperature is lowered, reaching a low-temperature value of $\sim 3.3e^2/h$, more than 80% of the maximum conductance $4e^2/h$, at 1.8 K. At higher bias, the conductance falls, due to electron scattering via emission of optical phonons.

The micrometer-scale scattering length for electrons at room temperature in metallic SWNTs is a striking result. The mean free path for electrons at room temperature in the best 3D metals, for example, copper, is on order tens of nanometers, due to phonon scattering. The difference arises from the 1D nature of the metallic SWNT. In one dimension, the phase space for scattering electrons is significantly reduced. Electrons may propagate only forward or backward in the nanotube, with a large momentum transfer required to backscatter the forward-moving electrons. This momentum is not present in any single acoustic phonon at room temperature. In three dimensions, electrons backscatter by undergoing a large number of small-angle collisions with acoustic phonons. Weak scattering has been predicted theoretically in metallic SWNTs (Anantram and Govindan 1998; White and Tudorov 1998; McEuen *et al*. 1999; Nakanishi and Ando 1999). McEuen *et al*. (1999) showed that the forward and backscattered electronic states in metallic SWNTs have opposite parity, and would require a short wavelength scattering potential to cause scattering. Nanotubes have also been shown to be relatively insensitive to point defect disorder: since the electronic states are extended over the circumference of the nanotube, point disorder is effectively averaged out (White and Tudorov 1998).

While the mean free path is orders of magnitude larger in metallic SWNTs than in traditional metals, the conductivity is only comparable or slightly better. This is due to the very low density of states in nanotubes, arising primarily from the semimetallic nature of graphene. There is a trade-off in 1D metals; the same low density of states allows the Peierls distortion to be pushed well below room temperature. A 1D system with significantly larger number of conducting modes per area would likely be a Peierls insulator at room temperature.

There are of course limits to the astounding conductivity of metallic SWNTs. While room temperature acoustic phonons cannot backscatter electrons, optic and zone-boundary phonons do have the necessary momentum. They are too high in energy ($hf \sim 150\,\text{meV}$) to be present at room tempererature and low V_{sd}. At high source–drain voltages, however, electrons can emit these phonons and efficiently backscatter. This leads to a dramatic reduction of the conductance at high biases, as was first reported by Yao *et al*. (2000). This can be readily seen in the data of Figure 5. The scattering rate grows linearly with V_{sd}, leading to a saturation of the total current through the SWNT. This saturation value is $\sim(4e^2/h)\, hf \sim 25\,\mu\text{A}$ for small diameter SWNT. This corresponds to a current density of $j = 2.5 \times 10^9\,\text{A/cm}^2$ for a 1 nm diameter tube—orders of magnitude larger than current densities found in present-day interconnects. Metal interconnects typically fail via electromigration. In covalently bonded carbon nanotubes, however, there are no low-energy defects or dislocations that can lead to migration of atoms. Nanotubes have been observed to carry current densities of $10^9\,\text{A/cm}^2$ for periods of weeks without failure (Wei *et al*. 2001).

b. Low Temperature: Coulomb Blockade

The low-temperature behavior of metallic SWNT devices depends strongly on the magnitude of the contact resistance, and a rich spectrum of behaviors has been observed. Electronic transport through devices with high resistance contacts will be dominated by Coulomb blockade at low temperature (Bockrath *et al.* 1997; Tans *et al.* 1997); the energy associated with adding an electron to the isolated nanotube island will exceed the thermal energy $k_B T$. If the contact resistance is very low, however, electrons will pass nearly freely into the nanotube from the leads. Small residual scattering at the two contacts will lead to interference and Fabry–Perot-like oscillations of the conductance of the nanotube (Liang *et al.* 2001). In the intermediate regime of contact resistance $R_c \leq h/e^2$, more exotic transport mechanisms, such as tunneling via the Kondo resonance, may be observed (Nygard *et al.* 2000). This section will focus primarily on the case of fairly resistive barriers, and the resulting Coulomb blockade, because of its application to single-electron tunneling devices.

A finite-sized metallic island has an associated charging energy $E_c = e^2/2C_\Sigma$ where C_Σ is the total capacitance of the island. The charging energy represents the electrostatic energy required to add a single electron to the island. If the island is well separated from its surroundings (i.e., the conductance of the contacts to the island $G_{\text{contact}} < e^2/\text{h}$) and the thermal energy $k_B T$ is much less than the charging energy E_c, then the charge on the island cannot fluctuate and hence current cannot be transported across the island. This is the Coulomb blockade.

In a single-electron transistor (SET), two leads are coupled to a small island through tunnel barriers, such that $G_{\text{contact}} < e^2/h$. A third gate electrode is coupled capacitively to the island. The total island capacitance is thus $C_\Sigma = C_l + C_r + C_g$, where C_l and C_r are the capacitances to the left and right leads, and C_g the capacitance to the gate electrode. In general, when $k_B T \ll E_c$ no current may pass from the left lead through the island to the right lead. However, if the electrochemical potential of the island can be tuned by a nearby gate electrode, the island will conduct whenever the n and $n+1$ electron states are degenerate. As the voltage on the gate electrode is changed, a charge $q = C_g V_g$ is induced on the island. Of course this charge must be added discretely, so the charge state of the island changes by one whenever $C_g V_g$ changes by and amount e. This gives rise to periodic oscillations in the conductance through the island as a function of gate voltage, with a period $\Delta V_g = e/C_g$.

For an SWNT device, it is found that the capacitance is simply proportional to length L; $C = L$ in cgs units. The charging energy E_c of the SWNT is approximately $3\,\text{eV}/L$, where L is measured in nanometers. This points out the importance of charging effects even for room temperature nanodevices; the charging energy will exceed room temperature for nanotube devices of

$L < 50\,\text{nm}$. Room temperature nanotube SETs will be discussed in greater detail below in Section V.2.

Experimentally, it is found that for metal-on-top devices L measures the length of the SWNT between electrodes (Bockrath *et al.* 1997) [see Fig. 2(a)]. In essence, although the SWNT extends underneath the electrode, its electronic structure is significantly perturbed by the metal electrode, and therefore it may be thought of as electronically "cut" at the edge of the metal electrode. For some tube-on-top devices, apparently the less strongly interacting contacts do not cut the SWNT, and L may represent the entire length of the SWNT (Tans *et al.* 1997) [see Fig. 2(b)].

An interesting property of SWNT SET devices is that even long SWNT islands may be *quantum dots* at low temperature; that is, the single-particle level spacing ΔE may exceed the thermal energy $k_B T$. For a 1D island, the single particle level spacing scales inversely with length: $\Delta E = \pi\hbar v_F/L$, where $\hbar$ is Planck's constant, and v_F is the Fermi velocity. For a metallic SWNT, $\Delta E \approx 0.5\,\text{eV}/L$ where L is measured in nanometers. Since the charging energy is also inversely proportional to length, the ratio of charging energy to level spacing $E_c/\Delta E$ is fixed. This is not true, in general, in one dimension; the inverse dependence on L comes from the linear dispersion at the Fermi surface, so only metallic SWNTs have a fixed $E_c/\Delta E$. The implication is that quantum effects will be important for any metallic SWNT SET device; because operation at temperatures $k_B T \ll E_c$, will necessitate $k_B T$ less than or approximately equal to ΔE.

The discreteness of the energy levels modifies the Coulomb blockade somewhat. The addition energy E_{add} for adding an electron to the quantum dot is now $E_{add} = e^2/C + \Delta E$, and the period of oscillations in V_g becomes

$$\Delta V_g = \frac{C_\Sigma}{eC_g}\left(\Delta E + \frac{e^2}{C_\Sigma}\right)$$

which reduces to $\Delta V_g = e/C_g$ in the limit $\Delta E \to 0$.

The presence of discrete energy levels in the SWNT quantum dot gives rise to additional features in the electronic transport (Bockrath *et al.* 1997; Tans *et al.* 1997, 1998a; Cobden *et al.* 1998b). This may be seen clearly by performing "transport spectroscopy" measurement of the differential conductance dI/dV as a function of both the source–drain voltage and gate voltage (Kouwenhoven *et al.* 1997). Such a transport spectroscopy measurement on a SWNT quantum dot is shown in Fig. 6.

The observation of discrete energy levels with spacing consistent with the length of the entire SWNT (Tans *et al.* 1997; McEuen *et al.* 1999) (up to 8 μm) in metallic tube-on-top devices indicates that at low temperature, electronic transport is coherent across the entire length of the SWNT, that is, the coherence length (and the mean free path) is at least 8 μm.

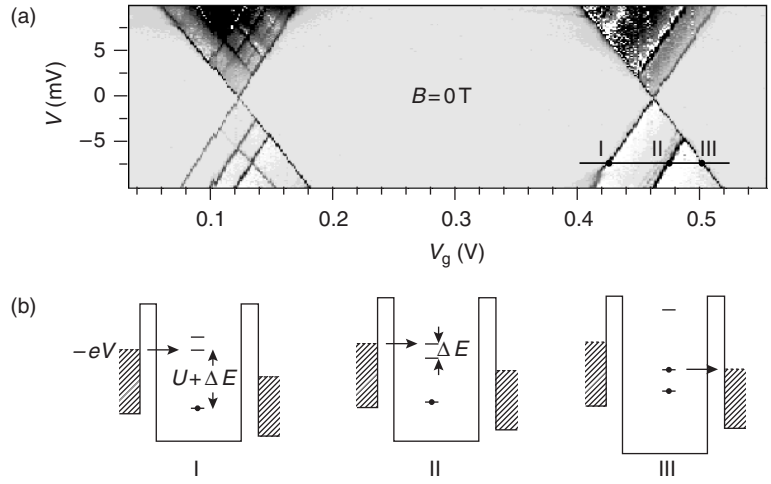

FIG. 6. Conductance spectroscopy of a metallic SWNT at 100 mK (Cobden *et al.* 1998b) (images courtesy of P. L. McEuen). The plots show the differential conductance (greyscale, dark is higher conductance) as a function of bias voltage V and gate voltage V_g for zero magnetic field (a) and a magnetic field of 5 T (b). The two points of finite conductance at zero bias voltage in (a) and (b) each represent the addition of one electron to the nanotube. The diagonal lines of finite conductance appear as states become available for tunneling within the source–drain bias window, as represented schematically in (c). As the gate voltage is increased [from points I to II to III in panel (a)], the single-particle states move down in energy as shown in (c). At point I, the addition of an electron from the left lead first becomes allowable, and a peak in the differential conductance occurs. At point II, an additional single-particle level becomes available for tunneling, and another peak in the differential conductance appears. At point III, the state corresponding to the added electron has moved below the potential of the right lead; beyond this point the current drops again, so another peak in differential conductance is seen. Application of a magnetic field (b) results in Zeeman splitting of some of the single-particle levels.

As discussed above, the two conditions necessary for Coulomb blockade are: (1) that the temperature be low enough such that $k_B T \ll E_c$; and (2) that the contacts are resistive such that $R_c \ll h/e^2$. The second condition is not necessarily true for nanotube devices—near ohmic contacts to nanotubes have been demonstrated (Kong *et al.* 2001; Liang *et al.* 2001). As the contact resistance is reduced, the charging energy is also reduced; E_c must go to zero as R_c goes to zero. This is indeed observed in nanotube devices (Liang *et al.* 2001). Suitable engineering of the contact resistance would allow for both ballistic and single-electron charging devices to be constructed from metallic SWNTs.

c. Temperature Dependence: Luttinger Liquid Tunneling

The conductance of high-contact-resistance metallic SWNT devices was observed to decrease as the temperature was lowered (Bockrath *et al.* 1999)

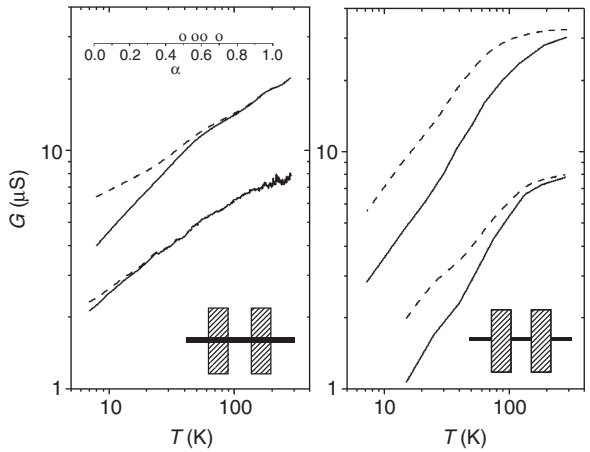

FIG. 7. The linear response (low-bias) conductance as a function of temperature for a tube-on-top device SWNT (left panel) and a metal-on-top SWNT device (right panel), showing power-law behavior due to Luttinger liquid tunneling (Bockrath *et al.* 1999). The solid lines are the measured data, the dashed lines are corrected for temperature dependence due to Coulomb blockade (Bockrath *et al.* 1999). The dashed lines show a power-law temperature dependence, in accordance with predictions for tunneling into a Luttinger liquid (see text). The inset in the left panel shows the exponents from the power-law dependence inferred from the data for several devices. Open circles denote metal-on-top devices, crosses denote tube-on-top devices.

(see Fig. 7). The zero bias conductance G varied as a power law in temperature T: $G(T) \sim T^{\alpha}$ (see Fig. 7). In addition, the differential conductance $\mathrm{d}I/\mathrm{d}V$ varied as a power law in bias voltage V: $\mathrm{d}I/\mathrm{d}V \sim V^{\alpha}$. The exponent α was the same in each case, but depended on the geometry of the device (metal-on-top vs tube-on-top).

As shown above in Section IV.2.a, the two-terminal conductance of a metallic nanotube device largely measures the contact properties. The results were interpreted in terms of electrons tunneling from metallic leads into a Luttinger liquid, the interacting ground state of a 1D metal (Fisher and Glazman 1997). The Luttinger liquid is characterized by a single parameter g, which measures the strength of the Coulomb interaction between electrons. In the non-interacting limit $g = 1$, while for strongly repulsive interactions, $g \ll 1$. For any system with $g \neq 1$, the elementary excitations of the system cannot be described as single-particle-like, and thus Fermi liquid theory breaks down.

The metallic SWNT is expected to have a value of g moderately less than unity (Egger and Gogolin 1997; Kane *et al.* 1997). For a finite length SWNT, the Luttinger liquid parameter is given by:

$$g = \left[1 + \frac{2E_{\mathrm{c}}}{\Delta E}\right]^{-1/2}$$

where E_c is the charging energy of the SWNT and ΔE is the single-particle energy level spacing. Experiments (Bockrath *et al.* 1997; Tans *et al.* 1997; Cobden *et al.* 1998a) give the ratio $E_c/\Delta E = 6$–10, which gives $g = 0.22$–0.28 (Bockrath *et al.* 1999); a theoretical estimate using a screening length of 1000 Å gives $g = 0.3$ (Kane *et al.* 1997).

Tunneling from a Fermi liquid into a Luttinger liquid is suppressed at low energy, since the tunneling electron must excite a packet of excitations in the Luttinger liquid. The tunneling conductance of the Luttinger liquid is predicted to follow a power law in both temperature and bias voltage $G(T) \sim T^{\alpha}$ and $dI/dV \sim V^{\alpha}$ (Bockrath *et al.* 1999) (see Fig. 7). The power-law exponent α depends on the number of 1D modes in the Luttinger liquid, and on the geometry of the tunnel junctions (whether the electron tunnels into the end or the bulk of the Luttinger liquid). For an SWNT with four conducting modes, it was found that:

$$\alpha_{\text{bulk}} = \frac{g^{-1} + g - 2}{8}$$

$$\alpha_{\text{end}} = \frac{g^{-1} - 1}{4}$$

$$\alpha_{\text{bulk-bulk}} = 2\alpha_{\text{bulk}} = \frac{g^{-1} + g - 2}{4}$$

$$\alpha_{\text{end-end}} = 2\alpha_{\text{end}} = \frac{g^{-1} - 1}{2}$$

where α_{bulk}, α_{end}, $\alpha_{\text{bulk–bulk}}$, and $\alpha_{\text{end–end}}$ are the power-law exponents for tunneling from electrode into the SWNT bulk, from electrode into the SWNT end, from the bulk of one SWNT to the bulk of another SWNT, and from one SWNT end to another SWNT end, respectively.

These four geometries have been realized experimentally. Tube-on-top SWNT devices act as bulk-contacted Luttinger liquids, while metal-on-top SWNT devices act as end-contacted Luttinger liquids (see Fig. 7). The other geometries, the bulk-to-bulk and end-to-end Luttinger liquids, were realized by Postma *et al.* (2000) by manipulating SWNTs using an AFM tip. A sharp kink in a SWNT formed a tunnel barrier, and thus an end-to-end contact, while the bulk-to-bulk contact was formed by cutting a SWNT with the AFM tip and then pushing the ends back together so they crossed. Experimentally, these geometries give $\alpha_{\text{bulk}} = 0.3$, $\alpha_{\text{end}} = 0.6$, $\alpha_{\text{bulk–bulk}} = 0.5$, and $\alpha_{\text{end–end}} = 1.4$. The Luttinger interaction parameters extracted from these four experiments using the formulas above are 0.24, 0.29, 0.26, and 0.27, respectively, in very good agreement with the theoretical prediction $g = 0.22$–0.28.

3. SEMICONDUCTING SINGLE-WALLED NANOTUBES

a. Two-Terminal Conductance at Room Temperature

Semiconducting behavior in SWNTs was first reported by Tans *et al.* (1998b). Figure 3(b) shows a measurement of the conductance of a semiconducting SWNT as the gate voltage applied to the conducting substrate is varied. The nanotube conducts at negative V_g and turns off with a positive V_g. The resistance change between the on and off state is many orders of magnitude. This device behavior is analogous to a p-type MOSFET, with the nanotube acting as the semiconductor channel. At large positive gate voltages, n-type conductance is sometimes observed, especially in larger-diameter nanotubes (Park and McEuen 2001; Javey *et al.* 2002). The conductance in the n-type region is typically less than in the p-type region because of the work function of the Au electrodes. The Au Fermi level aligns with the valence band of the SWNT, making a p-type contact with a barrier for the injection of electrons.

Semiconducting nanotubes are found to be doped slightly p-type; that is, the conductance is finite at $V_g = 0$. This arises because chemical species, particularly oxygen, adsorb on the tube and act as weak p-type dopants. Experiments have shown that changing a tube's chemical environment can change this doping level—shifting the voltage at which the device turns on by a significant amount (Bockrath *et al.* 2000; Kong *et al.* 2000a,b; Derycke *et al.* 2001). This has spurred interest in nanotubes as chemical sensors. The threshold voltage is very sensitive to the processing history of the device—for example, heating or exposure to UV radiation drives off oxygen, lowering the p-doping level of the device. Controlling adsorbate doping is an important challenge to be addressed. More will be said on this below in Section V.1.

In the data of Fig. 3(b), the conductance initially rises linearly with V_g as additional holes are added to the nanotube. At higher gate voltages, the conductance stops increasing and instead is nearly constant. This limiting conductance is presumably due to the contact resistance between the metallic electrodes and the nanotube. As with metallic SWNT devices, EFM measurements again may be used to determine the nature of the resistance (Fuhrer *et al.* 2001).

Figure 8 shows an EFM trace on a 4.5 μm long semiconducting SWNT grown by CVD. The voltage drop along this nanotube indicates a resistance of approximately 9.2 kΩ/μm. The mean free path l, the distance over which the transmission probability $T = \frac{1}{2}$, is given by the length over which the conductance is $4e^2/h$, or the resistance is ~6.5 kΩ. This gives $l = 700$ nm for this semiconducting SWNT at room temperature and zero gate voltage (only lightly p-doped) (Fuhrer *et al.* 2001).

During the EFM measurement, there is a large potential difference between the tip and the sample. The tip may therefore locally modify the

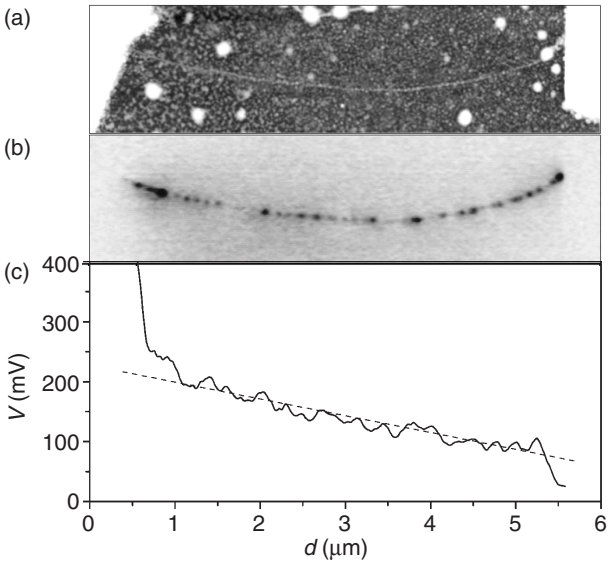

FIG. 8. EFM and SGM measurements of a semiconducting SWNT at room temperature (Fuhrer *et al.* 2001). A topographic AFM image is shown in (a); the white areas at left and right are the Cr/Au electrodes, and the faint gray line is the nanotube. An SGM image of the same device is shown in (b). The SGM image was taken with −1 V applied to the tip, and 1 V applied across the nanotube. Dark color indicates decreased resistance; black corresponds to a change in resistance of approximately 500 Ω. The local potential in the nanotube under an applied bias of 400 mV as measured by EFM is shown in (c). The dashed line is a guide to the eye, and represents a voltage drop corresponding to 9.2 kΩ/μm. The distance scale in (c) applies to all panels.

conducting properties of the sample as it scans over it; this is particularly likely in the case of the semiconducting nanotubes, since their conductance changes with shifts in the Fermi level. Scanned gate microscopy (SGM) images this perturbation by measuring the conductance of the sample as a function of tip position. The conductance changes when the tip locally depletes, or gates, the underlying electron system. This technique has been used in the past to study quantum point contacts (Eriksson *et al.* 1996) and quantum Hall conductors (Woodside *et al.* 2001).

Figure 8(b) shows an SGM image of a semiconducting SWNT device. The tip affects the conductance only at discrete locations along the nanotube. The resistance change at each point under application of a negative gate voltage is less than 1 kΩ, indicating each point is only weakly scattering the electrons; the intrinsic resistance arises from a large number of weakly scattering defects. These locations are likely areas of high local potential, caused by disorder in the nanotube or defects, for example, trapped charge, in the substrate (Fuhrer *et al.* 2001).

Unlike in metallic SWNTs, the intrinsic resistance of semiconducting SWNT is strongly dependent on the synthesis method and treatment of the nanotube material. Previous EFM measurements on semiconducting SWNTs derived from the laser ablation process and deposited on substrates after ultrasonication show that large barriers to transport ($R_i \sim M\Omega$) are present along the nanotube with a spacing of order ~ 100 nm (Bachtold *et al.* 2000).

The mean free path may be used to estimate the carrier mobility for the semiconducting nanotube. The mobility is given by $\mu = e\tau/m^* = el/m^* v_F$, where the τ is the scattering time and m^* is the effective mass of the holes. For a 1D conductor with two bands at the Fermi level, $m^* v_F = \hbar k = \pi\hbar n/4$ where $\hbar$ is Planck's constant and n the hole density per unit length. The hole density may be estimated from the capacitance per length c_g, using $n = c_g(V_t - V_g)$, where V_t is the threshold voltage. The capacitance per unit length of the tube can be obtained from low temperature measurements of metallic SWNT (Bockrath *et al.* 1997; Tans *et al.* 1997; Cobden *et al.* 1998b). Using $c_g = 6.0\,e^-/V \cdot \mu m$, and $V_t - V_g \approx 10$ V, a mobility $\mu = 23\,000\,cm^2/V \cdot s$ is obtained.

The transport data $G(V_g)$ [see Fig. 3(b)] may also be analyzed to extract a carrier mobility. The Drude conductivity relation $\sigma = ne\mu$, where σ is the conductivity and n the linear carrier density, predicts that the conductance of the nanotube will grow linearly with carrier density (and hence gate voltage) if the mobility is constant: $G = c_g(V_t - V_g)\mu/L$. From the linear portion of the $G(V_g)$ curve a mobility of the tube μ may be inferred. For the 4.8 μm long semiconducting SWNT device in Fig. 3(b), the slope $dG/dV_g = 2.2\,\mu S/V$. Using a capacitance of $c_g = 6.0\,e^-/V \cdot \mu m$, a mobility $\mu = 11\,000\,cm^2/V \cdot s$ is obtained.

Typical mobilities for CVD-grown SWNTs obtained from the $G(V_g)$ characteristics are in the range of a few thousand to occasionally as high as $20\,000\,cm^2/V \cdot s$. Mobility determined from $G(V_g)$ may underestimate the true mobility if the contact resistance also varies with gate voltage, which is not unreasonable. The fact that the EFM measurements are consistent with the highest mobilities from $G(V_g)$ bears this out.

These mobilities significantly exceed the mobilities of laser-ablation nanotubes deposited from suspension, where μ is on order 10–100 $cm^2/V \cdot s$ (Martel *et al.* 1998). The mobilities of CVD-grown semiconducting SWNTs are extraordinary, exceeding the best room temperature Si MOSFETs, indicating that SWNTs are a remarkably high-quality semiconducting material.

b. Low Temperature

Initial low-temperature experiments were performed on laser-ablation derived SWNT. Transport spectroscopy performed on such semiconducting

SWNT devices shows a large gap in the conductance as a function of source–drain voltage at positive V_g which narrows at negative V_g, but never closes. This behavior has been interpreted as follows: at positive V_g, the semiconducting SWNT is depleted of carriers and the barrier to transport is the intrinsic bandgap. At negative V_g, the SWNT contains hole carriers, but disorder causes the SWNT to break up into a string of quantum dots in series separated by large barriers (McEuen *et al.* 1999). Because the dots are in series, at any given V_g some of the dots will be blockaded and there will be a gap to transport. The size of the gap (25–50 meV) indicates that the smallest dots are on order 100 nm. This is consistent with the observation via EFM of large barriers to transport along the length of the nanotube (Bachtold *et al.* 2000).

More recently, devices have been made using semiconducting SWNTs grown via CVD. At low temperature, and at negative gate voltage, a single oscillation period of the conductance as a function of gate voltage is seen, similar to metallic SWNT quantum dots (Fuhrer *et al.* 2001). The period in V_g and charging energy are consistent with a quantum dot with the length of the entire semiconducting SWNT, in this case $\sim$1 μm. This indicates a mean free path of at least 1 μm at low temperature; implying that if semiconducting SWNTs are made relatively free of disorder, they may also have long mean free paths at low temperature.

No reports have to date been made of ohmically contacted semiconducting SWNTs. This may indicate the presence of an intrinsic barrier at the semiconducting SWNT–electrode interface, at least for the electrodes currently being employed. It is also not clear how to apply the model of Luttinger liquid tunneling to the semiconducting nanotubes. The contact resistance of semiconducting nanotubes does increase as the temperature is lowered, but connection with the Luttinger tunneling model is greatly complicated by the nonlinear band dispersion and the closeness of the Fermi level to the band edge.

4. SUMMARY OF ELECTRONIC TRANSPORT PROPERTIES

Nanotubes are extremely 1D; a 1.5 nm SWNT has a sub-band spacing of order 1 eV, much greater than the room temperature thermal energy of 25 meV. Because of the 1D nature of carbon nanotubes, electronic transport properties must be interpreted carefully. For instance, a perfect (zero scattering) SWNT with perfect contacts will still have a two-terminal resistance of $\sim$6.5 kΩ, the quantized contact resistance of a 1D channel with four modes.

The interacting ground state of a 1D conductor is termed the Luttinger liquid. The excitations of the Luttinger liquid are no longer single-particle-like. This has consequences for the conductance of a tunnel junction

contact to a SWNT; a power-law gap is observed in the tunnel conductance as a function of voltage and temperature.

The intrinsic resistance of the SWNT channel may be much less than the measured two-probe resistance. Metallic SWNTs have mean free paths of $>1\,\mu m$, while moderately doped semiconducting SWNTs have mean free paths of hundreds of nanometers. These values correspond to resistances of <6 and $\sim 10\,k\Omega/\mu m$ for metallic and semiconducting SWNTs, respectively. The resistivities of nanometer-diameter metallic and semiconducting SWNTs are on order $10^{-6}\,\Omega\,cm$, comparable to good metals.

Given the dispersionless nature of the metallic SWNT bands, and some uncertainty in how to define the carrier density (relative to the sub-band bottom or band bottom), it is difficult to assign a mobility to the metallic SWNT devices. For semiconducting nanotubes, there is a well-defined effective mass and carrier density is readily defined relative to the bandgap edge; thus the mobility can be defined. Furthermore, a fairly linear dependence of the conductance on gate voltage (and hence the carrier density n) also argues for the usefulness of the mobility in describing the properties of semiconducting nanotubes; over a significant range, the carrier mobility is constant and the conductivity is Drude-like, increasing linearly with n. Semiconducting nanotubes have extraordinary room temperature mobilities, reaching values up to $20\,000\,cm^2/V \cdot s$, exceeding high-mobility Si MOSFETs.

V. Nanotube Nanoelectronic Devices

This section will discuss efforts to fabricate useful electronic devices based on carbon nanotubes. The fundamental motivation for this work is the impending end of Moore's law scaling in silicon CMOS electronics. This has motivated a great deal of interest in the search for alternative technologies that may replace or augment CMOS. Such technologies generally come under the heading "nanoelectronics", since the relevant length scale at which they will become competitive with CMOS is thought to be significantly less than 100 nm.

Many nanoelectronics schemes have in common the idea of "bottom-up" assembly. In contrast to "top-down" assembly, where circuits are laid out precisely and then shrunk to sub-micrometer dimensions using, for example, lithography, "bottom-up" assembly starts with individual nanometer-scale components, and uses weak forces, for example, molecular recognition, to "self-assemble" the components into some useful larger structure. The hope is that the significant drawbacks of self assembly (high defect density, simplicity of structure) will be overcome by its advantages (small component size, low cost).

At first glance, nanotubes seem an ideal material for bottom-up fabrication: both metals and semiconductors are present, nanotubes are extremely robust to chemical and physical treatment, and carbon chemistry is well known. However, significant hurdles exist which have yet to be addressed: no method exists for separating nanotubes according to electronic property; solubility of nanotubes is poor; and while organic carbon chemistry is well known, graphene chemistry is not. Efforts to overcome these difficulties will be discussed in the next section.

Nevertheless, work on nanoelectronic nanotube devices progresses. Out of necessity, the first model devices have been constructed using a top-down approach. These include nanotube FETs and SETs, the basics of which were discussed in Section IV. This section will continue the discussion with greater focus on tailoring the characteristics of these devices to produce useful behavior.

One of the simplest geometries which may be considered in a bottom-up fabrication scheme is a grid of perpendicular wires, often called a crossbar array. The fabrication of such a grid only requires the fabrication of an array of aligned, evenly spaced long wires (twice, at right angles to each other). Devices in the crossbar array may be formed naturally at the junctions between wires (the wires are the devices), or may be placed at the junctions through further self-assembly (the wires are the interconnects). In either case, electronic programmability of devices is a useful characteristic, since this allows the use of the use of the very simple geometry to create more complicated devices. Nanotube–nanotube junctions have been explored as both electronic and programmable electromechanical devices as well as robust nanoscale interconnects.

1. FIELD-EFFECT TRANSISTORS

As discussed in Section IV.3, the semiconducting SWNT channel acts like an FET; positive gate voltage shuts off conduction, while the conduction is enhanced by negative gate voltage. Because the field is rapidly developing, it is worthwhile to briefly review the history of the attempts to understand the device behavior of SWNT FETs before continuing to discuss efforts to modify that device behavior.

Tans *et al.* (1998b) reported the first electrical transport measurements on an individual semiconducting SWNT, as discussed in Section IV.3.a. Their devices were made using laser ablation derived SWNT material using the tube-on-top method. Tans *et al.* considered that the semiconducting SWNT acts as an intrinsic *ballistic* channel between the source and drain electrodes. Because of difference in work function ϕ between the metal electrodes (platinum, with a work function $\phi = 5.7\,\text{eV}$) and the nanotube (with $\phi = 4.5\,\text{eV}$), the Fermi level in the nanotube is pinned in the valence band at

the contacts. Far from the electrodes, the nanotube is intrinsic. The bands bend towards the intrinsic position over the electrostatic screening length, which may be very long in one dimension. This creates a barrier for hole transport through the nanotube, which may be lowered by applying a negative voltage to the gate electrode. The analogous semiconductor device is termed a barrier impact transit time (BARITT) diode. Since the barrier height depends strongly on the ratio of the device length to the electronic screening length, the BARITT model predicts a large sensitivity of the device characteristics to device length, which was not observed in subsequent research.

Martel *et al.* (1998) also fabricated semiconducting SWNT devices from laser ablation derived material using the tube-on-top technique. They observed similar device characteristics as reported by Tans *et al.*, but explained the transistor behavior with a qualitatively different model: conduction through the semiconducting SWNT is *diffusive*. The semiconducting SWNT acts as the channel of a MOSFET, apparently intrinsically doped slightly p-type, and the device operates in a p-channel depletion mode (positive gate voltage shuts off the conduction, and negative gate voltage enhances the conduction). The conductance saturates at large negative V_g due to the series resistance of the contacts. The linear region in the conductance as a function of gate voltage was used to extract a hole mobility with a rather low value of $20\,cm^2/V \cdot s$.

As discussed above, scanned probe experiments (see Section IV.3) shed light on this problem. Electronic transport through laser ablation derived semiconducting SWNTs is dominated by a number of large conductance barriers (Bachtold *et al.* 2000), which explains the low mobility of the devices measured by Martel. *et al.* In CVD-grown semiconducting SWNTs, the intrinsic resistance is much lower; the mean-free path is several hundred nanometers, and the hole mobility may be as high as $20\,000\,cm^2/V \cdot s$. However, the transport is still diffusive, as seen from EFM experiements (Fuhrer *et al.* 2001), and semiconducting SWNT devices have a well-defined resistance per length.

a. Transconductance

As discussed in Section IV.3.a, the conductance of an FET is given by $G = c_g(V_t - V_g)\mu/L$. The transconductance dI_{SD}/dV_g is then maximized by increasing the gate capacitance and the carrier mobility. The transconductances of the first SWNT FETs were very low, simply because most experiments to date have used gate oxide thicknesses of hundreds of nanometers. More recently, researchers have investigated a number of ways to increase the gate coupling. Bachtold *et al.* (2000) deposited SWNTs on top of oxidized Al wires which acted as gate electrodes. In this way FETs were constructed

with dielectric thicknesses of a few nanometers. Although low-mobility laser ablation derived SWNTs were used, transconductances of up to 0.3 μS were obtained, and transistor–resistor logic devices showing gain were constructed.

An electrolytic solution may be used to gate CVD-grown semiconducting nanotube devices (Rosenblatt *et al.*, unpublished results) (see Fig. 9). In this way the effective dielectric thickness could be made very small, on the order of a few nanometers. A maximum transconductance of 20 μS was observed. Normalizing this to the device width of ~2 nm, this gives a transconductance per unit width of ~10 mS/μm; significantly better than current-generation MOSFETs, but reasonable in light of the high hole mobility of semiconducting SWNTs.

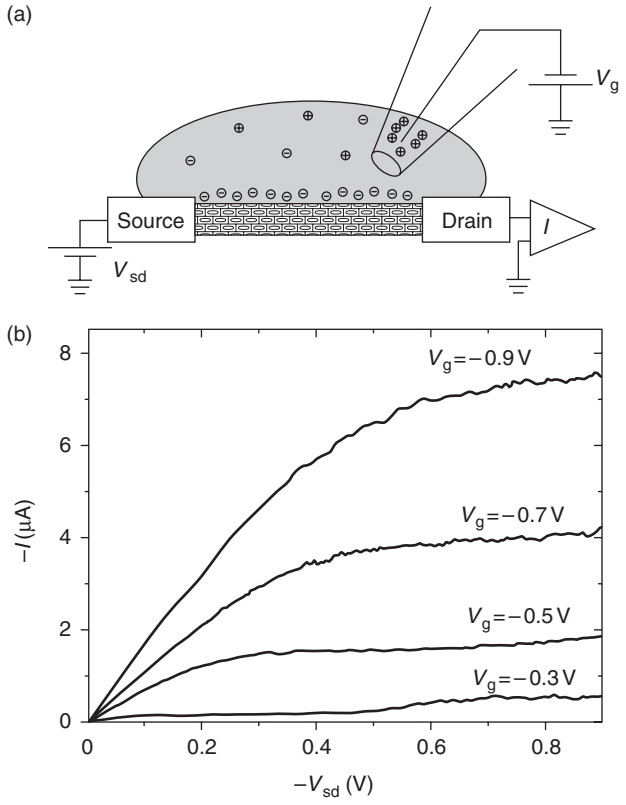

FIG. 9. Gating an SWNT FET using an ionic solution (images courtesy P. L. McEuen). A schematic of the device is shown in (a). A pipette containing a NaCl solution (1–100 mM) is used to place a drop of solution over the device. An electrode inside the pipette acts as a gate terminal. The device chartacteristics are shown in (b). The maximum transconductance of the device is 20 μS.

b. Doping

As-prepared semiconducting SWNT FETs are normally-on (depletion mode) p-channel FETs. The p-channel conduction results from pinning of the Fermi level of the SWNT at the electrode at or near the valence band edge, and normally-on behavior results from doping by ambient species such as oxygen. Control of the nanotube-electrode interface, and control of the chemical doping of the nanotube channel may be used to alter these characteristics.

n-Type doping of SWNTs was first accomplished using alkalai metals that donate electrons to the tube. This has been used to create n-type transistors (Bockrath *et al*. 2000; Kong *et al*. 2000a; Derycke *et al*. 2001), p–n junctions (Zhou *et al*. 2000), and p–n–p devices (Kong *et al*. 2002). Alkalai metals are not air-stable, however, so other techniques are under development, such as using polymers for charge-transfer doping (Kong and Dai 2001).

Martel *et al*. (2001) found that annealing of nanotubes with titanium electrodes forms a covalently bonded TiC–nanotube contact, with the Fermi level in the SWNT at the interface pinned near the center of the gap. The hole doping due to oxygen could be removed by passivating the device with SiO_2, followed by treatment at high temperature. After this process, ambipolar transistor behavior is observed, with efficient injection of both electrons and holes. This is intriguing, because typically the sum of the Schottky barrier heights for electrons and holes should equal the band gap ($\sim$600 meV for the laser ablation derived nanotubes used in this study). Apparently once electrons or holes are induced into the bulk of the SWNT, the Schottky barrier width in the 1D nanotube becomes extremely small, so tunneling through the barrier dominates the conduction.

c. Summary

The high mobility of semiconducting SWNTs leads to excellent device properties in SWNT FETs. While the first devices had low transconductances due to poor quality nanotubes and extremely thick gate dielectrics, recent experiments indicate that, with a suitably thin gate dielectric, the transconductance of SWNT FETs may exceed that of the best silicon devices when scaled by the device dimensions. Work on doping the nanotube channel and controlling the nanotube–metal interface has progressed significantly. n-Type doping has been demonstrated, and ambipolar transistor action has been achieved by using covalently bonded TiC contacts to the nanotube.

Several unique aspects of the nanotube FET have been pointed out as possible advantages for applications. Unlike conventional MOSFETs, the conducting channel of the nanotube FET is exposed at the surface. High sensitivity of the nanotube FET to chemical environment has already been

demonstrated, and it is natural to think of the applicability of nanotube FETs as chemical sensors. SWNT FETs can operate in water, including in ionic solutions, suggesting possible sensing applications in a biological or chemical "lab on a chip". The small size of the nanotube FET suggests memory applications; the use of SWNT FETs in floating-gate memories could reduce the amount of stored charge, and greatly increase speed and density.

2. SINGLE-ELECTRON TRANSISTORS

Since the first SETs were fabricated by Fulton and Dolan (1987) in 1987, there have been efforts to increase the operating temperature for single-electron devices. There now exist a handful of reports on SETs operating at room temperature. Room temperature SETs have been fabricated by nano-oxidation of a Ti metal film using a scanned-probe tip (Matsumoto *et al.* 1996), random oxidation to form constrictions in a thin silicon wire (Zhuang *et al.* 1998), and even using the original technique of Fulton and Dolan (electron-beam lithography and shadow evaporation to form $Al/AlO_x/Al$ structures) by modifying the electron-beam lithography to achieve exceedingly fine resolution (Pashkin *et al.* 2000). A charging energy of over 150 meV was reported for an SET using a single C_{60} molecule as an island, but the device was not shown to be operable at room temperature (Park *et al.* 2000).

Since the capacitance of SWNT SETs scales inversely with length (see Section IV.2.b) one may predict that a SWNT device with length shorter than $\sim$50 nm will have a charging energy greater than the thermal energy at room temperature. Lefebvre *et al.* (2000) fabricated very short SWNT SETs via a metal-on-top technique, with the gap between electrodes defined by a nanotube used as a shadow mask. They found an electron addition energy in their devices on order 100 meV, but no Coulomb oscillations were observed at room temperature, possibly due to thermal activation of electrons over the tunnel barrier formed at the nanotube–electrode interface.

Postma *et al.* (2000) had shown that tunnel junctions could be produced in metallic SWNTs through AFM manipulation to produce a kink (see also Section IV.2.c). Bozovic *et al.* (2001) took advantage of this technique to produce pairs of tunnel junctions in SWNTs to form SETs with island sizes less than 100 nm. These small islands acted as SETs. One island with length $\sim$50 nm had an addition energy of $\sim$70 meV, and showed Coulomb oscillations up to a temperature of about 165 K. Postma *et al.* (2001) used the double-kink technique to produce a device with a length of $\sim$25 nm, which showed Coulomb oscillations at room temperature (see Fig. 10). This device had an addition energy of $\sim$120 meV.

The AFM manipulation technique used to fabricate double-kink SWNT SETs is rather uncontrollable, and difficult to envision as a method of mass production. However, these devices show in general some of the advantages

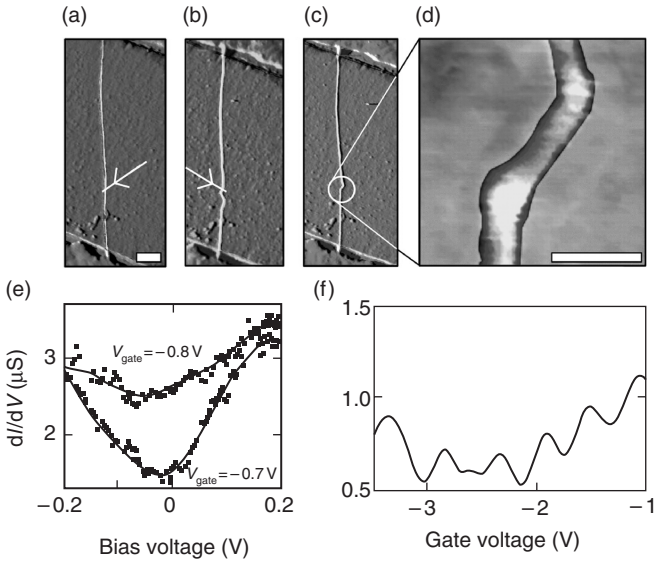

FIG. 10. Room temperature nanotube SET (Postma *et al.* 2001) (images courtesy Cees Dekker). An AFM tip was used to modify a nanotube device by dragging over the device along the lines shown in (a) and (b). This formed two kinks in the nanotube shown in (c) and (d). The scale bar in (a)–(c) is 200 nm, and the scale bar in (d) is 20 nm. The differential conductance as a function of bias voltage (e) at 300 K shows significant variation with gate voltage. The differential conductance as a function of gate voltage (f) at 260 K shows periodic oscillations due to Coulomb blockade.

of making SETs from SWNTs, which in principle may be generalized to other fabrication techniques.

The reason that scaling of the SWNT SETs to small lengths produces high charging energy devices is that the capacitance is dominated by the length of the nanotube, not the area of the contacts. In SETs fabricated by, for example, the $Al/AlO_x/Al$ process the total capacitance is typically dominated by the capacitance of the tunnel junctions. In order to produce smaller capacitance devices, one must make smaller area tunnel junctions (Pashkin *et al.* 2000). The problems with this approach are that fabricating small tunnel junctions by brute-force lithography is extremely difficult, and the resistance of the tunnel junction increases as the area decreases. With SWNT SETs, a small-area tunnel junction is self-assembled; the area of the SWNT controls the area of the junction. Lithography need only define the long dimension of the SET, on the order of 25 nm for room temperature operation.

This advantage may also be seen in the ratio of gate capacitance to total capacitance C_g/C_Σ for the SWNT SETs. Both double-kink devices discussed above have ratios of C_g/C_Σ of around 0.3, while the room temperature SET described by Pashkin *et al.* has a ratio C_g/C_Σ of about 3×10^{-3}, two orders of

magnitude smaller. That this ratio determines the maximum transconductance of an SET can be shown by a rough calculation as follows: The transconductance is the change in current through the device divided by the change in gate voltage. The maximum current modulation will be produced if the device operates at a source-drain bias $V_{sd} \approx E_c = e/2C_\Sigma$. The maximum possible conductance through a single-electron charging device is $G_{max} \approx e^2/h$. Thus, the maximum possible current is $I_{max} = G_{max}V_{sd} = e^3/2hC_\Sigma$. The current varies from minimum to maximum over a change in gate voltage $\Delta V_g/2 = e/2C_g$. Therefore, the transconductance is $2I_{max}/\Delta V_g \approx (e^2/h)(C_g/C_\Sigma)$. This simple derivation assumes that the device is classical, that is, $\Delta E \ll k_B T$, which is not true for the SWNT devices. However, the general result holds, increasing C_g/C_Σ increases the transconductance of the device.

The result above suggests that not only would SWNT islands make good SETs, but metal islands with SWNT leads would also make good SETs, since they too would have small junction capacitances.

3. NANOTUBE HETEROJUNCTION DEVICES

a. Linear Nanotube Heterojunctions

Iijima observed discrete transitions in the curvature of the shells making up MWNTs, and posited that the insertion of a pentagon or heptagon in the graphene lattice was responsible (Iijima 1993). It was pointed out that nanotubes of different diameter and/or chirality may be joined seamlessly by the introduction of pairs of pentagons and heptagons into the graphene lattice (Dunlap 1994). All carbon metal–semiconductor diodes were envisioned by joining a metallic and a semiconducting SWNT by a single pentagon–heptagon pair (Charlier *et al.* 1996; Chico *et al.* 1996; Saito *et al.* 1996). Chico *et al.* (1998) explored the possibility of an on-tube quantum dot produced by a pair of pentagon–heptagon defects which connected a metallic (5,5) SWNT to two semiconducting (6,4) SWNT leads.

Collins *et al.* (1997) provided the first experimental hints at the existence of on-nanotube electronic devices. They probed a tangled mat of laser ablation produced SWNT bundles with an STM tip. The tip was brought into electrical contact with the mat, and it was found that the tip could often be retracted for several micro meters before electrical contact was lost. They proposed a model of a sliding contact between tip and nanotube bundle as the tip was retracted. During retraction of the tip, current–voltage (I–V) characteristics of the tip–mat junction were acquired at various retraction distances. It was found that the I–V characteristics would sometimes abruptly change from symmetric to strongly rectifying. These events were interpreted as the tip sliding past a defect in a nanotube which acted as an on-tube device. The experiments of Collins *et al.* were performed essentially

blind; the STM was not used in imaging mode. Hence, there was no direct evidence that the rectifying behavior resulted from an on-tube device, and not, for example, a junction between two different SWNTs in a bundle, or a shift of the STM tip from one SWNT to another in a bundle.

In fabricating tube-on-top electrical devices (see Section III.2), Yao *et al.* (2000) occasionally observed individual SWNTs with sharp kinks along their length. Out of 500 devices, four were found with single kinks, and one with two kinks. These kinks were interpreted as individual pentagon–heptagon pair defects causing an abrupt change of chirality of the SWNT at the defect. Electrical measurements on two kinked SWNTs were reported in detail. The first device unfortunately spanned only three electrodes, so independent two-terminal measurements could only be performed on one side of the kink. The portion of the nanotube on this side of the kink junction had a two-probe conductance of 110 kΩ, with no gate voltage dependence, indicating a metallic SWNT. Two-probe measurements across the kink, however, gave an immeasurably low conductance (<4 pS) at zero bias, but a strong non-linear onset of conduction when around +1–2 V was applied to the metallic SWNT. The onset of conduction shifted significantly with the application of a gate voltage, becoming more conducting at positive bias for negative gate voltages. Because of the gate voltage dependent conductivity of the kink segment, the side of the kink which contact only a single electrode was presumed to be a semiconducting SWNT. The rectifying behavior was then attributed to the formation of a metal–semiconductor Schottky barrier at the kink, although the very high threshold voltage (1–2 V) (Odintsov 2000) and the incorrect sign of the rectification (a Schottky barrier between a metal and p-doped semiconductor should conduct for negative bias applied to the metal) indicated that the device may be somewhat more complicated. (A second device was found to be a junction between two metallic SWNTs; the conductance of this device was consistent for an end-to-end Luttinger liquid junction as discussed in Section IV.2.c.)

b. Nanotube T and Y Junctions

More complex all-carbon covalently bonded nanotube structures have also been envisioned (Hamada 1993; Menon and Srivastava 1997). Hamada studied the band structure of 1D, 2D, and 3D superstructures formed by the joining of SWNTs with pentagons and heptagons, and envisioned an all-carbon circuit network. Menon and Srivastava (1997) studied two T junctions connecting metallic and semiconducting SWNTs. The junctions were shown to be stable under molecular dynamics relaxation. Andriotis *et al.* (2001) found that Y junctions between SWNTs may rectify currents.

Such ideal junctions between SWNT have been difficult to realize experimentally. However, a number of authors have reported branching

structures of larger tubular carbon nanofibers, synthesized by templated pyrolysis of acetylene in nanochannel alumina (Li *et al*. 1999), pyrolysis of nickelocene and thiophene (Satishkumar *et al*. 2000), pyrolysis of methane over cobalt supported on MgO (Li *et al*. 2001), and pyrolysis of methane over iron particles on roughened silicon (Ting and Chang 2002). These structures are all tens of nanometers in diameter and thus not electronically one dimensional at room temperature. Moreover, those structures for which TEM images exist show poor graphitization (Li *et al*. 1999, 2001; Satishkumar *et al*. 2000), and thus do not fit the strict definition of nanotube used in this chapter. However, electrical measurements of individual examples as well as ensembles of Y junction fibers synthesized inside nanochannel alumina templates show interesting rectifying behavior, though it is difficult to connect these structures with the rectifying Y junctions considered theoretically (Andriotis *et al*. 2001).

c. Crossed-Nanotube Junctions

Devices consisting of single junctions between individually electrically contacted nanotubes have been fabricated using a metal-on-top method (Fuhrer *et al*. 2000). Each crossed-SWNT device consisted of two crossed individual SWNTs or small bundles (diameter < 3 nm) of SWNTs with four electrical contacts, one on each end of each SWNT or bundle. The inset of Fig. 11 shows an AFM image of such a crossed nanotube device; two crossed SWNTs interconnect Cr/Au contacts.

This configuration allows each SWNT in the junction to be measured independently to determine its properties. The room temperature two-terminal conductance as a function of gate voltage $G(V_g)$ characteristics measured across the individual SWNTs allowed for the assignment of each as metallic or semiconducting. Each crossed-SWNT device can be composed of two metallic SWNTs (MM), one metallic and one semiconducting SWNT (MS), or two semiconducting SWNTs (SS).

Figure 11 shows the four-terminal current–voltage (I–V) characteristic of an MM junction at 200 K (filled squares). The slope of the I–V curve corresponds to a resistance of 200 kΩ, or a conductance of $0.13e^2/h$. Similar measurements of three other MM junctions gave conductances of $0.086e^2/h$, $0.12e^2/h$, and $0.26e^2/h$. The measurements of SS junctions are often complicated by the presence of high resistance barriers in the laser-ablation synthesized semiconducting SWNT (see Section IV.3). Nevertheless, two-terminal conductances of SS junctions as high as $0.011e^2/h$ and $0.06e^2/h$ (the higher conductance curve is represented by the filled circles in Fig. 11) were observed.

The measured conductances of MM junctions correspond to a transmission probability for the junction $T_j = G/(4e^2/h) \approx 0.02$–$0.06$. Thus, an

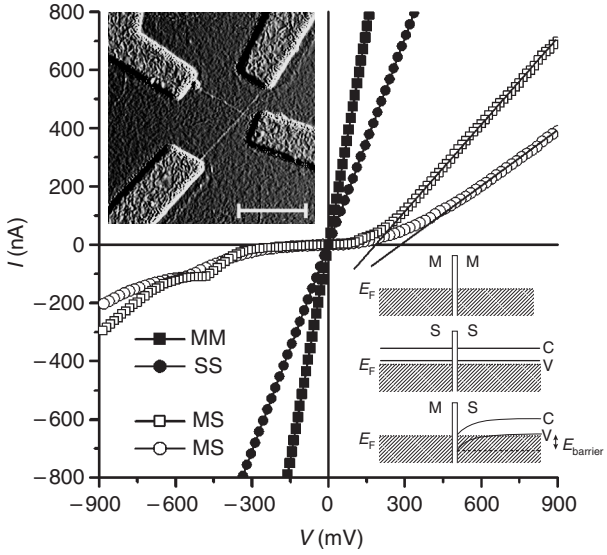

FIG. 11. Current–voltage characteristics of crossed carbon nanotube junctions (Fuhrer *et al.* 2000). The *I–V* curves of a metal–metal junction (filled squares), a semiconductor–semiconductor junction (filled circles), and two metal–semiconductor junctions (open squares and circles) are shown. The lower right inset shows the expected band profiles on either side of the junction for each case. The non-linear behavior of the metal–semiconductor junctions is due to the formation of a Schottky barrier at the junction, as shown in the inset. The solid lines in the main panel extrapolate the forward bias region to zero current, giving an estimate of the barrier height of 190–290 meV. The upper left inset show an AFM image of a typical crossed nanotube device. Two narrow crossing lines are SWNTs, the larger blocks are Cr/Au electrodes. The scale bar is 1 μm.

electron arriving at the junction in one SWNT has a few percent chance of tunneling into the other SWNT. MM junctions make surprisingly good tunnel contacts, despite the extremely small junction area on the order of 1 nm^2. In order to understand these results, first-principles density functional calculations of the conductance of MM junctions were performed. For two (5,5) SWNTs separated by the van der Waals distance of 0.34 nm, a transmission $T_j \approx 2 \times 10^{-4}$ was found. However, when the contact force between the nanotubes due to interaction with the SiO_2 substrate was included (Hertel *et al.* 1998), the nanotubes deformed significantly at the junction. In this case, it was found $T_j \approx 0.04$, in excellent agreement with the experimental result. The high conductance of MM junctions indicates that metallic SWNT junctions may be useful for branching interconnects.

The MS case is qualitatively different from the MM and SS cases. Charge transfer at the junction between a doped semiconducting SWNT and a metallic SWNT is expected to form a Schottky barrier (Odintsov 2000) with the Fermi level E_F of the metallic SWNT aligned with the center of the band

gap of the semiconducting SWNT at the junction (see lower inset, Fig. 11). The total barrier transmission probability T_{MS} is then given by $T_{MS} \approx T_j\, T_d$, where T_d is the transmission probability for tunneling through the depletion region to the location of the metal SWNT and T_j is the probability of tunneling between the SWNTs. $T_{MS} \approx 2 \times 10^{-4}$ for both MS devices in Fig. 11. If we assume that $T_j \approx 0.04$ for the MS junctions (comparable to the MM value), then $T_d \approx 5 \times 10^{-3}$, in excellent agreement with a calculation by Odintsov (2000), who found $T_d \approx 5 \times 10^{-3}$ and a corresponding depletion width of 7 nm for a doping level similar to the experimental case.

A Scottky barrier should also show asymmetric transport; indeed this is the case for the MS junction barrier (see Fig. 11). The V-intercept of the linear positive-bias region gives a gross measure of the barrier height: $E_{barrier} = 190$ and 290 meV for the two devices. This agrees reasonably well with the expected barrier height $E_{barrier} = E_g/2 \sim 250$–350 meV for 1–1.5-nm semiconducting SWNTs ($E_g \sim 500$–700 meV).

Poor rectification is obtained because the MS Schottky barrier is rather leaky. Better rectification was achieved with a three-terminal device which takes advantage of the double-width depletion barrier in the semiconducting nanotube (Fig. 12). A voltage was applied to one end of the semiconducting SWNT in an MS device, while the other end was grounded through a current-measuring amplifier. If the metal SWNT as well as one end of the semiconducting SWNT are grounded, the barrier to holes will remain intact

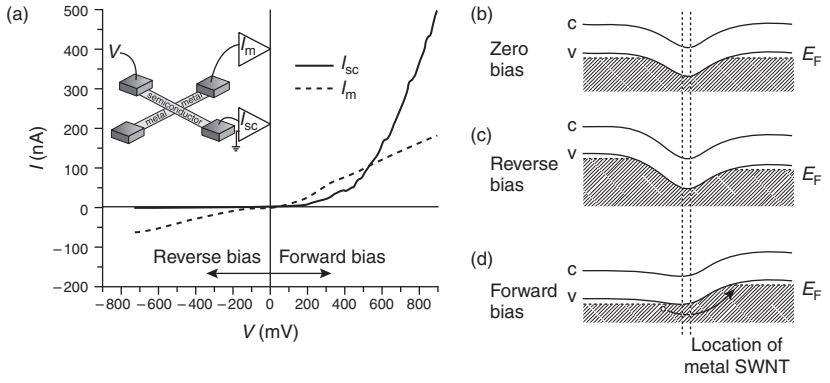

FIG. 12. Three-terminal characteristics of a metal–semiconductor crossed-nanotube junction (Fuhrer *et al.* 2000). In (a), the bias is applied to one end of the semiconducting nanotube, the current flowing to ground is measured at the other end (see inset). The metallic nanotube is also grounded through a current amplifier. The solid curve in (a) shows the current in the semiconducting nanotube as a function of bias voltage. The dotted curve shows the current flowing from the metallic nanotube. The schematic operation of the device is shown in (b)–(d). At zero bias (b), a depletion barrier exist in the semiconducting nanotube on either side of the metallic nanotube. On reverse bias (c), the barrier on the biased side increases, and no current flows. On forward bias (d), the barrier on the biased side is decreased, and holes may pass the barrier.

when a negative voltage is applied, because the metallic SWNT remains at roughly the same potential as the grounded end of the semiconducting SWNT [Fig. 12(c)]. However, when a positive bias is applied such that the potential difference between the metallic and semiconducting SWNT is greater than the barrier height, holes may pass the barrier, and current will flow through the semiconducting SWNT [Fig. 12(d)]. Such a response is observed in the measured current leaving the semiconducting SWNT [I_S in Fig. 12(a)].

The current from the semiconducting SWNT is approximately 100 times greater for a bias of +700 mV than for −700 mV. It has been noted that the ineffective screening inherent to 1D systems poses problems for nanotube Schottky devices (Leonard and Tersoff 1999): nanometer-scale depletion regions are likely to be leaky barriers to tunneling. This three-terminal device points out at least one solution to this problem; a good rectifier is constructed from narrow Schottky barriers. The active length of this device is on the order of 15 nm, demonstrating that useful devices consisting of only a few thousands of atoms can be constructed from SWNTs.

4. MECHANICAL DEVICES

Carbon nanotubes are exceedingly light and stiff. This suggests that nanomechanical devices based on carbon nanotubes could operate at very high speeds. Indeed, simple oscillators made from sub-micro meter nanotube beams have characteristic mechanical frequencies in the Gigahertz range (Reulet *et al*. 1999). In addition, nanotubes are exceptionally tough; the elastic limit (elongation) for SWNTs is ~6%. Nanotubes may be bent through large angles, and even buckled, and return to their original shape elastically (Yakobson and Avouris 2001). This suggests that nanotube mechanical devices could operate reversible for large numbers of cycles with no fatigue.

Rueckes *et al*. have proposed a mechanically bistable nanotube device which would act as a memory or programmable logic element (Rueckes *et al*. 2000). The device consists of two nanotubes; one lies on a substrate, while the other nanotube crosses it, suspended above it at a distance of a few nanometers (see Fig. 13). The total energy of the device was analyzed as a function of the nanotube separation for a range of initial separations and nanotube lengths, and bistability of the device was found for a broad range of parameters. The two stable states correspond to the nanotubes in close contact (held by van der Waals forces), and relaxed. In order to switch between the two states, opposite polarity voltages would be applied between the two nanotubes to cause them attract each other while like polarity voltage (relative to a third gate electrode) would cause the nanotubes to separate.

Rueckes *et al*. fabricated a demonstration device using bundles of SWNT deposited onto pre-fabricated gold electrodes with a height of 150 nm and a

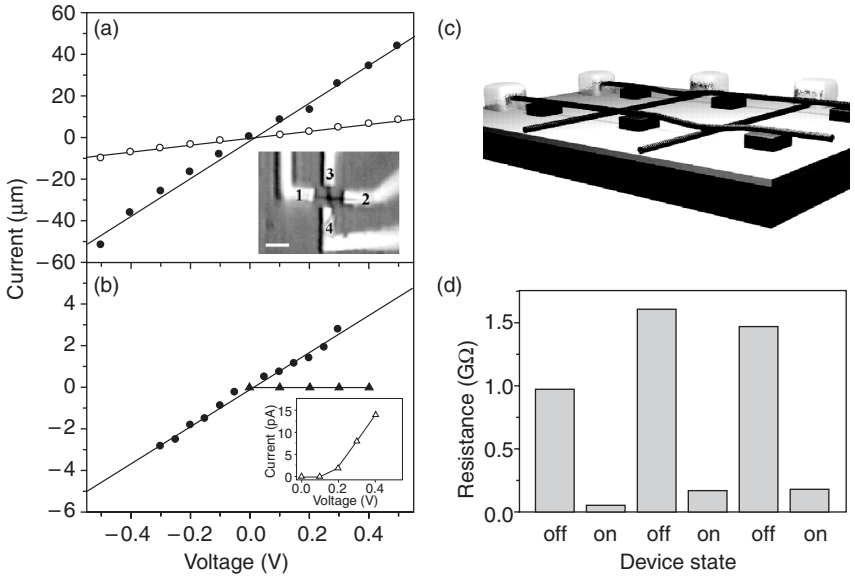

FIG. 13. Carbon nanotube mechanical memory (Rueckes *et al.* 2000) (images courtesy C. M. Lieber). The inset of (a) shows an optical micrograph (scale bar 4 μm) of a device consisting of two crossing bundles of SWNTs (dark lines) deposited on 150 nm high Cr/Au electrodes (white). The *I–V* characteristics measured from contacts 1 to 2 (solid circles) and 3 and 4 (open circles) are shown in (a). The *I–V* curves of the junction in the OFF state (open triangles) and ON state (solid circles) are shown in (b). The junction was switched to the ON state by the application of ±2.5 V. The schematic of a possible nanotube mechanical memory array is shown in (c). Panel (d) shows the ON/OFF resistance for a device similar to that shown in (a), but which showed reversible switching. This device could be switched ON with application of ±5 V, and OFF at 40 V.

separation of ~4 μm (see Fig. 13). They were able to demonstrate irreversible switching of one device from a separated state (>10 GΩ) to a contacted state (112 kΩ) at a voltage of 2.5 V. Another device switched reversibly from separated (1.36 GΩ) to contacted (140 MΩ) with the application of ±5 V to contact and 40 V to separate the SWNT bundles. The authors calculate that in principle, bistable devices could be made as small as 5–20 nm, with switching speeds of 100–200 GHz.

5. NANOTUBE INTERCONNECTS

Nanometer-scale integrated electronic devices will require enormous demands on interconnects. The power density dissipated by such devices will be tremendous; in ballistic devices this power will be dissipated in the

interconnects. Interconnects must be low resistance not only to reduce power consumption, but to increase device speed.

Nanotubes are excellent candidates for interconnects given their low electrical and thermal resistance, and stability at high temperature and current. As shown in Section IV.2.a, the resistivity of metallic single-walled carbon nanotubes is on order $10^{-6}\,\Omega\,\mathrm{cm}$, comparable or superior to copper. Furthermore, the conduction of electrons is quasi-ballistic; the energy of hot electrons is dissipated on a length scale exceeding many micro meters. Nanotubes may be used as exceedingly fine interconnects to nanoscale devices, for example in a crossbar geometry, in which molecular-sized devices are located at the junctions between crossing wires in an array. The ballistic nature of electron transport in nanotubes would allow the power to be dissipated far from the devices in macroscopic metal wires.

Even if longer nanotube interconnects are employed, such that the electron energy relaxes within the nanotube, the very high thermal conductivity and excellent thermal stability of nanotubes suggests that they would be superior to conventional metals. The phonon thermal conductivity of carbon nanotubes has been measured to be approximately 2000 W/m/K at room temperature, comparable to diamond, the best-known room temperature thermal conductor (Kim *et al.* 2001).

The current-carrying capacity of a single SWNT is limited by optical phonon emission to about $2.5 \times 10^9\,\mathrm{A/cm^2}$ for a 1 nm diameter tube—orders of magnitude larger than current densities found in present-day interconnects. Moreover, metal interconnects typically fail via electromigration. Electromigration should be enormously reduced in covalently bonded carbon nanotubes—there are no low-energy defects or dislocations that can lead to migration of atoms. Nanotubes have been observed to carry current densities of $10^9\,\mathrm{A/cm^2}$ for periods of weeks without failure (Wei *et al.* 2001).

VI. Outlook for Nanotubes in Nanoelectronics

As evidenced above, nanotube electronic devices have demonstrated some very attractive properties: high-speed, high-sensitivity FETs for memories, sensors, or logic circuits; high-transconductance SETs operating at room temperature; densely packed junction devices; robust, high-speed mechanical devices; and low-loss interconnects. However, significant roadblocks stand in the way of developing any of these devices for use in a technology.

In order for nanotube devices to find a home in an electronic technology, two major obstacles must be overcome: nanotubes must be prepared with uniform electronic properties, and methods must be found to place individual nanotubes precisely on a substrate. Any nanoelectronics technology faces similar versions of these challenges; however it is worth discussing some

of the problems that will be specific to nanotubes, and some of the efforts that have been made toward solving these problems.

There are two approaches to nanotube synthesis for electronic devices. In the first, large quantities of nanotubes are synthesized "off-chip", processed, then precisely placed on substrates using self-assembly techniques. In the second technique, nanotubes are grown "on chip" from specific sites on a substrate, and guided in specific directions through the use of, for example, electric fields. Both approaches face hurdles, but the nature of the hurdles is somewhat different in each case.

In the off-chip synthesis, the major challenge is to produce a physically and electronically uniform product that is soluble, so that self-assembly techniques such as chemical recognition can be used to precisely place the nanotubes on suitably prepared substrates. The holy grail of off-chip synthesis would be two vials of nanotubes; one containing a stable solution of metallic SWNTs of fixed length and diameter, another semiconducting SWNTs of fixed length and diameter. At this point, nanotubes would be analogous to any other component of "molecular electronics" and could be treated the same way; the hope being that the chemical self-assembly techniques will be developed to place molecule-sized objects with precision on substrates.

On-chip synthesis attempts to combine the self-assembly and synthesis in order to remove some of the intermediate processing. Here, the major challenge is to produce a suitable catalyst which under the proper conditions will produce a nanotube with uniform electronic properties. All that remains, then, is to self-assemble these catalyst particles into the desired positions, and then perform the growth procedure.

1. UNIFORMITY OF PROPERTIES

The unique "size effect" in carbon nanotubes—that the band structure changes enormously, from metal to semiconductor, with tiny changes in diameter and chirality—presents both a significant opportunity and a significant challenge. The opportunity is to realize a complete electronic system using only covalently bonded carbon networks. The challenge is that such structures must be constructed perfectly—small changes in the components will have drastic changes in the electronic properties.

There are several possible solutions to this challenge. One possibility is to enormously overbuild devices, and then remove unwanted components. For example, working transistors have been made from bundles containing both metallic and semiconducting SWNTs by first depleting the semiconducting nanotubes of carriers using a gate voltage, and then destroying the metallic nanotubes with a large voltage pulse (Collins *et al*. 2001). Another solution to the challenge would be the synthesis or extraction of a nanotube material that

is electronically uniform. This section will address some of the large body of research that has focused on this solution. (A third possibility—to find a new material that has some of the advantageous properties of carbon nanotubes, but is electronically uniform—will be discussed in Section VII.)

Smalley *et al.* synthesized SWNT with a narrow diameter distribution via laser ablation and concluded that the majority of the SWNT were metallic (10,10) nanotubes (Thess *et al.* 1996); the consensus is now that this was not the case. However, research continues toward finding a synthesis route to produce nanotubes of a single structure. Recently, small bundles of nanotube were synthesized via a novel method; layers of nickel and C_{60} were alternately evaporated onto a molybdenum surface through small apertures, followed by annealing at 950°C in vacuum and a magnetic field of 1.5 T (Schlittler *et al.* 2001). Small rods protruding from the substrate were found to be *crystals* of hundreds of nanotubes, each with identical diameter and helicity, although these parameter varied from crystal to crystal. It remains to be seen whether this technique can be scaled to produce large quantities of uniform nanotubes.

Controlling the uniformity of nanotubes has also been a challenge in chemical vapor deposition growth. Typically CVD-grown nanotubes are more heterogeneous than laser ablation derived nanotubes; presumably because of difficulties in making the catalyst particles monodisperse. Various research groups have attacked this issue. The iron-storage protein ferritin was used to produce uniform-size catalyst particles consisting of $\sim$200 or $\sim$1100 Fe atoms (Li *et al.* 2001). These catalyst particles were then used to grow nanotubes with diameters of 1.5 ± 0.4 and 3.0 ± 0.9 nm, respectively. Similar results were obtained with discrete-sized iron nanoparticles synthesized in solution; particles with average diameters of 3, 9, and 13 nm were used to grow nanotubes of average diameter 3, 7, and 12 nm (Cheung *et al.* 2002).

Barring the synthesis of uniform nanotubes, the extraction of nanotubes of a particular type from bulk sample is a desirable goal. The first step in such a scheme is solubilization of the nanotubes, then hopefully differences in their electrical, magnetic, structural, or chemical properties may be used to separate them via chromatography, electrophoresis, or selective chemical functionalization.

Solubilization of carbon nanotubes has, however, remained a major challenge, although a number of important steps in this direction have been taken. Nanotubes have been systematically shortened and suspended in surfactant solutions (Liu *et al.* 1998), where they may be purified via chromatography (Niyogi *et al.* 2001), although this procedure causes damage to the nanotube sidewalls. The damage, however, can allow functionalization of the sidewalls which can aid in solubility (Chen *et al.* 1998, 2001; Riggs *et al.* 2000). Nanotubes have also been rendered soluble by fluorination (Mickelson *et al.* 1998).

2. SELF-ASSEMBLY

Once nanotubes are solubilized, self-assembly schemes can be utilized to place them with precision on substrates. Such schemes rely on localized forces, such as chemical recognition or local electric fields, to guide the nanotubes into place. Shortened SWNTs exhibit sidewall carboxyl groups that have been used as the basis of functionalization, and the science of nanotube sidewall chemistry is proceeding rapidly.

Liu *et al*. were able to take advantage of the sidewall functionalization to place nanotubes precisely on substrates (Liu *et al*. 1999). They prepared SiO_2 substrates with a methyl-terminated self-assembled monolayer (SAM), to which it was observed that shortened SWNTs had poor adhesion. This monolayer was locally removed via electron beam radiation, and subsequently replaced with an amine-terminated SAM. When the substrate was exposed to a suspension of shortened SWNTs, the nanotubes stuck preferentially on the exposed areas. However, a few nanotubes were observed on areas outside the exposure. Electronic devices made by this method also showed poor electrical properties, probably due to the presence of sidewall defects.

VII. Beyond Carbon Nanotubes

An alternative solution to the problem of non-uniform electronic properties in carbon nanotubes is to find a material that is more electronically uniform, but still retains some of the advantageous properties of carbon nanotubes. Immediately after the discovery of carbon nanotubes, the possibility of synthesizing tubular structures of other layered materials was realized, and now a number of examples exist; the most well characterized being the $B_xC_yN_z$ system and the transition-metal dichalcogenides, both discussed below. Crystalline nanowires are another possible system. The vapor–liquid–solid reactions used to produce nanotubes of carbon may be generalized to a broad range of materials. Nanowires, however, lack the unique property of nanotubes that the surface states are eliminated.

1. INORGANIC NANOTUBES

Following the analogy of constructing nanotubes from single sheets of graphite, one may consider nanotubes of other layered compounds. Indeed, the synthesis of nanotubes from several other layered compounds has been reported.

The single sheet of hexagonal boron nitride (h-BN) is probably the closest analog to graphene; h-BN may be thought of as the III–V analog of graphite.

The inversion symmetry that allows a crossing of the π and π^* bands at the Fermi level is removed in h-BN, and consequently h-BN is a wide gap semiconductor, with $E_g = 5.8\,\text{eV}$ (Zunger *et al.* 1976). Nanotubes of h-BN were predicted to be stable and be semiconducting with large band gaps (Rubio *et al.* 1994); for tube larger than $\sim$1 nm the band gap is fairly constant (on order 5.5 eV), tending towards the bulk value for large diameters (Blase *et al.* 1994).

Soon after the prediction of their stability, multiwalled h-BN nanotubes were indeed synthesized, by arc discharge between a BN-packed tungsten rod and a copper electrode (Chopra *et al.* 1995). Following this discovery, both single and multi-walled h-BN nanotube have been produced by a variety of methods (Golberg *et al.* 1996; Loiseau *et al.* 1996; Weiqiang *et al.* 1998; Yu *et al.* 1998; Cummings and Zettl 2000). The synthesis techniques have been refined, and now highly pure monodisperse single-wall (Lee *et al.* 2001) and, intriguingly, double-wall (Cummings and Zettl 2000) h-BN nanotubes have been produced. Still, electronic conduction properties of h-BN nanotubes have not been reported; it remains unclear whether these large band gap semiconducting nanotubes will be useful for electronics.

Perhaps more intriguing electronically are other nanotubes from the $B_xC_yN_z$ family. Besides BN, there exist other $B_xC_yN_z$ analogs of graphite that form stoichiometric structures; for example BC_2N and BC_3 (Krishnan *et al.* 1988). Nanotubes of BC_2N were considered theoretically (Miyamoto *et al.* 1994a). Two possible structures for the BC_2N sheet were considered, with one structure leading to metallic or semiconducting behavior dependent on chirality (similar to the carbon nanotube case) and the other giving only semiconducting behavior, with a moderate gap of $\sim$1.3 eV. The second case is particularly interesting; since these nanotubes were formed from a sheet which possesses a strongly anisotropic structure, chiral nanotubes could be envisioned in which the current-carrying states may have an angular momentum about the tube axis (Miyamoto *et al.* 1996, 1999).

Nanotubes of BC_3 have also been considered theoretically (Miyamoto *et al.* 1994b), and found to have a lower formation energy compared to the sheet than similar-diameter carbon nanotubes, suggesting their stability. Band structure calculations show metallic or small gap ($\sim$0.2 eV) semiconducting character, tending to uniformly small gap semiconducting at larger diameters.

Arcing a composite rod of BN and graphite indeed produced multiwalled nanotubes (Weng-Sieh *et al.* 1995); within the same sample individual nanotubes were identified by electron energy-loss spectroscopy (EELS) performed in a TEM as being stoichiometrically BC_2N and BC_3. Arcing a hafnium diboride rod together with a graphite rod in a nitrogen atmosphere produced intriguing structures of B, C, and N (Suenaga *et al.* 1997). Multiwalled nanotubes and onion-like nanoparticles were observed with adjacent walls of pure C and pure BN. One particular MWNT studied by EELS in a

TEM had 14 walls; the inner three were carbon, the next six BN, and the outer five were again carbon. Such structure have led to fanciful description of nano-coaxial cables, however, no electrical transport results have been reported.

Layered transition-metal dichalcogenides have also been explored as a basis for constructing nanotubes. These materials consist of layers three atoms thick; a single layer of transition metal capped on either side by layers of sulfur, selenium, or tellurium. These three atom thick layers are weakly bound together through van der Waals interactions. Molybdenum disulfide is perhaps the most familiar example, finding use as a dry lubricant. Both WS_2 and MoS_2 nanotubes have been synthesized in significant quantities (Tenne and Zettl 2001). Typically, the results are large MWNTs. However, it was recently reported that crystals of monodisperse SWNTs of MoS_2 with diameter of 0.96 nm could be produced in large quantities, raising interest in these nanotubes as electronic nanowires with uniform properties (Remskar *et al*. 2001). Similar to these MoS_2 nanotubes, crystals of chains of Mo_3Se_3 with width of $\sim$0.6 nm have been prepared (Hornbostel *et al*. 1995). These fibers are soluble in polar solvents, and electrical measurements on single fibers show that they are conducting at room temperature (Venkataraman and Lieber 1999).

2. SEMICONDUCTOR NANOWIRES

It has been known for over 30 years that narrow crystalline wires of silicon may be prepared through a vapor–liquid–solid reaction with a metal catalyst, for example gold (Wagner and Ellis 1964); however, the technique was limited by the size of the catalyst particles to produce wires of $>$100 nm diameter (Wagner 1970). By analogy to the laser ablation production of nanotubes, silicon and other semiconductor nanowires may be produced by laser ablation of a catalyst-containing target; small particles of catalyst are formed in the ablation plume, and nanowires grow via a VLS reaction (Morales and Lieber 1998; Zhang *et al*. 1998). Crystalline semiconductor nanowires may also be grown from solid-supported nanoparticle catalysts (Yazawa *et al*. 1992; Westwater *et al*. 1997) and via solution–liquid–solid reactions (Trentler *et al*. 1995; Holmes *et al*. 2000). Crystalline nanowires of elemental semiconductors (e.g., Si, Ge), and compounds (e.g., GaAs, GaN, InP) have been prepared; given the universality of the Vapor–Liquid–Solid reaction, the possible list of nanowires which may be prepared is very large.

Many of the advances in fabricating electronic devices from semiconductor nanowires have come from the Lieber group at Harvard. Their approach has been to form devices at the crossing junctions of nanowires. Aligned nanowire arrays have been self-assembled by deposition from a suspension flowing through a microchannel over a substrate (Huang *et al*. 2001a).

Arrays of crossed nanowires may be obtained by sequential deposition of more nanowires at an angle to the first array. In this way, a number of crossed nanowire devices may be formed. Silicon nanowires doped p- and n-type with boron or phosphorus were found to make rectifying junctions. Junctions between p-type silicon and n-type GaN nanowires could act as either diodes, or, after oxidation of the silicon nanowire, FETs (Huang *et al.* 2001b).

Crystalline semiconductor nanowires have a number of possible advantages over carbon nanotubes; the electronic properties as well as processing techniques of inorganic semiconductors are already well understood, their electronic properties may be controlled through doping (Cui *et al.* 2000), and they may be oxidized controllably to form barriers (Cui and Lieber 2001). However, because of the high doping levels and large numbers of surface states, it is unlikely the nanowires will achieve the high conductivities or high mobilities demonstrated in nanotube FETs. The current state of self-assembly and integration of nanowire devices is, however, more advanced compared to nanotube devices. Given the similarity to existing semiconductor technology in materials processing and device behavior, semiconductor nanowires may be a model system to study nanoscale devices produced by self-assembly.

VIII. Conclusions

Interest in carbon nanotubes for nanoelectronics was sparked by the theoretical prediction of a 1D conductor that was impervious to the Peierls distortion, and whose electronic properties could be tuned through changes in atomic structure. Nanometer-diameter SWNTs have since been mass produced, and are indeed metallic or semiconducting depending sensitively on their diameter and helicity. Experiments have since revealed a material that has exceeded all expectations: metallic SWNTs rival the best metals in conductivity at room temperature, and semiconducting SWNTs have room temperature mobilities comparable to the best semiconductors.

A range of electronic devices have been demonstrated which exploit the unique properties of carbon nanotubes. Nanotube FETs have transconductances per width that rival the best silicon FETs. Nanotube SETs operate at room temperature due to natural nanometer-size low-capacitance junctions. Junctions between nanotubes demonstrate the ultimate in small: working two- and three-terminal devices containing a few thousand atoms that can rectify microampere currents. Nanotube interconnects carry current densities of greater than 10^9 A/cm^2 for extended periods of time without failure.

These devices are proofs of the principle that useful nanoelectronic devices can be constructed from nanotubes. However, they certainly do not represent

a technology; each was painstakingly constructed one by one using slow serial fabrication techniques. The challenge now lies in engineering. No techniques yet exist for the mass production of electronically uniform nanotube materials, or the placement of those nanotubes precisely into electronic circuits. However, the advances in the past 5 years since the first SWNT devices were constructed have been enormous. There is every reason to expect that the next 5 years will be equally productive.

REFERENCES

Anantram, M. P., and T. R. Govindan, Conductance of carbon nanotubes with disorder: a numerical study, *Phys. Rev. B (Condens. Matter)* **58**, 4882 (1998).

Andriotis, A. N., M. Menon, D. Srivastava, and L. Chernozatonskii, Rectification properties of carbon nanotube "Y-junctions", *Phys. Rev. Lett.* **87**, 066802 (2001).

Bachtold, A., M. S. Fuhrer, S. Plyasunov, M. Forero, E. H. Anderson, A. Zettl, and P. L. McEuen, Scanned probe microscopy of electronic transport in carbon nanotubes, *Phys. Rev. Lett.* **84**, 6082 (2000).

Bandow, S., A. M. Rao, K. A. Williams, A. Thess, R. E. Smalley, and P. C. Eklund, Purification of single-wall carbon nanotubes by microfiltration, *J. Phys. Chem. B* **101**, 8839 (1997).

Bethune, D. S., C. H. Kiang, M. S. Devries, G. Gorman, R. Savoy, J. Vazquez, and R. Beyers, Cobalt-catalysed growth of carbon nanotubes with single-atomic-layer walls, *Nature* **363**, 605 (1993).

Bezryadin, A., A. R. M. Verschueren, S. J. Tans, and C. Dekker, Multiprobe transport experiments on individual single-wall carbon nanotubes, *Phys. Rev. Lett.* **80**, 4036 (1998).

Blase, X., A. Rubio, S. G. Louie, and M. L. Cohen, Stability and band gap constancy of boron nitride nanotubes, *Europhys. Lett.* **28**, 335 (1994).

Bockrath, M., D. H. Cobden, P. L. McEuen, N. G. Chopra, A. Zettl, A. Thess, and R. E. Smalley, Single-electron transport in ropes of carbon nanotubes, *Science* **275**, 1922 (1997).

Bockrath, M., D. H. Cobden, L. Jia, A. G. Rinzler, R. E. Smalley, L. Balents, and P. L. McEuen, Luttinger-liquid behaviour in carbon nanotubes, *Nature* **397**, 598 (1999).

Bockrath, M., J. Hone, A. Zettl, P. L. McEuen, A. G. Rinzler, and R. E. Smalley, Chemical doping of individual semiconducting carbon-nanotube ropes, *Phys. Rev. B (Condens. Matter)* **61**, R10606 (2000).

Bozovic, D., M. Bockrath, J. H. Hafner, C. M. Lieber, P. Hongkun, and M. Tinkham, Electronic properties of mechanically induced kinks in single-walled carbon nanotubes, *Appl. Phys. Lett.* **78**, 3693 (2001).

Charlier, J. C., P. Lambin, and T. W. Ebbesen, Electronic properties of carbon nanotubes with polygonized cross sections, *Phys. Rev. B (Condens. Matter)* **54**, R8377 (1996).

Chen, J., M. A. Hamon, H. Hu, Y. Chen, A. M. Rao, P. C. Eklund, and R. C. Haddon, Solution properties of single-walled carbon nanotubes, *Science* **282**, 95 (1998).

Chen, J., A. M. Rao, S. Lyuksyutov, M. E. Itkis, M. A. Hamon, H. Hu, R. W. Cohn, P. C. Eklund, D. T. Dolbert, R. E. Smalley, and R. C. Haddon, Dissolution of full-length single-walled carbon nanotubes, *J. Phys. Chem. B* **105**, 2525 (2001).

Cheung, C. L., A. Kurtz, H. Park, and C. M. Lieber, Diameter-controlled synthesis of carbon nanotubes, *J. Phys. Chem. B* **106**, 2429 (2002).

Chico, L., V. H. Crespi, L. X. Benedict, S. G. Louie, and M. L. Cohen, Pure carbon nanoscale devices: nanotube heterojunctions, *Phys. Rev. Lett.* **76**, 971 (1996).

Chico, L., M. P. Lopez Sancho, and M. C. Munoz, Carbon-nanotube-based quantum dot, *Phys. Rev. Lett.* **81**, 1278 (1998).

Chopra, N. G., R. J. Luyken, K. Cherrey, V. H. Crespi, M. L. Cohen, S. G. Louie, and A. Zettl, Boron nitride nanotubes, *Science* **269**, 966 (1995).

Cobden, D. H., M. Bockrath, P. L. McEuen, A. G. Rinzler, and R. E. Smalley, Spin splitting and even-odd effects in carbon nanotubes, *Phys. Rev. Lett.* **81**, 681 (1998).

Cobden, D. H., M. Bockrath, N. G. Chopra, A. Zettl, P. L. McEuen, A. Rinzler, A. Thess, and R. E. Smalley, Transport spectroscopy of single-walled carbon nanotubes, *Physica B* **251**, 132 (1998a).

Collins, P., A. Zettl, H. Bando, A. Thess, and R. Smalley, Nanotube nanodevice, *Science* **278**, 100 (1997).

Collins, P. G., M. S. Arnold, and P. Avouris, Engineering carbon nanotubes and nanotube circuits using electrical breakdown, *Science* **292**, 706 (2001).

Cui, Y., and C. M. Lieber, Functional nanoscale electronic devices assembled using silicon nanowire building blocks, *Science* **291**, 851 (2001).

Cui, Y., X. Duan, J. Hu, and C. M. Lieber, Doping and electrical transport in silicon nanowires, *J. Phys. Chem. B* **104**, 5213 (2000).

Cumings, J., and A. Zettl, Mass-production of boron nitride double-wall nanotubes and nanococoons, *Chem. Phys. Lett.* **316**, 211 (2000).

Dai, H., A. G. Rinzler, P. Nikolaev, A. Thess, D. T. Colbert, and R. E. Smalley, Single-wall nanotubes produced by metal-catalyzed disproportionation of carbon monoxide, *Chem. Phys. Lett.* **260**, 471 (1996).

Datta, S., *Electronic Transport in Mesoscopic Systems*, Cambridge University Press, Cambridge (1995).

Dekker, C., Carbon nanotubes as molecular quantum wires, *Phys. Today* **52**, 22 (1999).

Derycke, V., R. Martel, J. Appenzeller, and P. Avouris, Carbon nanotube inter- and intramolecular logic gates, *Nanoletters* **1**, 453 (2001).

Dunlap, B. I., Relating carbon tubules, *Phys. Rev. B (Condens. Matter)* **49**, 5643 (1994).

Egger, R., and A. O. Gogolin, Effective low-energy theory for correlated carbon nanotubes, *Phys. Rev. Lett.* **79**, 5082 (1997).

Eriksson, M. A., R. G. Beck, M. Topinka, J. A. Katine, R. M. Westervelt, K. L. Campman, and A. C. Gossard, Cryogenic scanning probe characterization of semiconductor nanostructures, *Appl. Phys. Lett.* **69**, 671 (1996).

Fisher, M. P. A., and A. Glazman, *Mesoscopic Electron Transport*, Kluwer Academic, Boston, MA (1997).

Forró, L., and C. Schönenberger, Physical properties of multi-wall nanotubes, in *Topics in Applied Physics*, edited by M. S. Dresselhaus, G. Dresselhaus, and P. Avouris, Vol. 80, Springer, Berlin, p. 329 (2001).

Fuhrer, M. S., J. Nygård, L. Shih, M. Forero, Y.-G. Yoon, M. S. C. Mazzoni, H. J. Choi, J. Ihm, S. G. Louie, A. Zettl, and P. L. McEuen, Crossed nanotube junctions, *Science* **288**, 494 (2000).

Fuhrer, M. S., M. Forero, A. Zettl, and P. L. McEuen, Ballistic transport in semiconducting carbon nanotubes, in *Electronic Properties of Molecular Nanostructures*, edited by H. Kuzmany, J. Fink, M. Mehring, and S. Roth, AIP Conference Proceedings, New York, p. 401 (2001).

Fulton, T. A., and G. J. Dolan, Observation of single-electron charging effects in small tunnel junctions, *Phys. Rev. Lett.* **59**, 109 (1987).

Golberg, D., Y. Bando, M. Eremets, K. Takemura, K. Kurashima, and H. Yusa, Nanotubes in boron nitride laser heated at high pressure, *Appl. Phys. Lett.* **69**, 2045 (1996).

Hafner, J. H., M. J. Bronikowski, B. R. Azamian, P. Nikolaev, A. G. Rinzler, D. T. Colbert, K. A. Smith, and R. E. Smalley, Catalytic growth of single-wall carbon nanotubes from metal particles, *Chem. Phys. Lett.* **296**, 195 (1998).

Hafner, J. H., C. Chin-Li, T. H. Oosterkamp, and C. M. Lieber, High-yield assembly of individual single-walled carbon nanotube tips for scanning probe microscopies, *J. Phys. Chem. B* **105**, 743 (2001).

Hamada, N., Electronic band structure of carbon nanotubes: toward the three-dimensional system, *Materials Science & Engineering B* **19**, 181 (1993).

Hamada, N., S. Sawada, and A. Oshiyama, New one-dimensional conductors—graphitic microtubules, *Phys. Rev. Lett.* **68**, 1579 (1992).

Hertel, T., R. E. Walkup, and P. Avouris, Deformation of carbon nanotubes by surface van der Waals forces, *Phys. Rev. B (Condens. Matter)* **58**, 13870 (1998).

Holmes, J. D., K. P. Johnston, R. C. Doty, and B. A. Korgel, Control of thickness and orientation of solution-grown silicon nanowires, *Science* **287**, 1471 (2000).

Hornbostel, M. D., S. Hillyard, J. Silcox, and F. J. DiSalvo, Nanometer width molybdenum selenide fibers, *Nanotechnology* **6**, 87 (1995).

Huang, Y., M. Okada, K. Tanaka, and T. Yamabe, Estimation of Peierls-transition temperature in metallic carbon nanotube, *Solid State Commun.* **97**, 303 (1996).

Huang, Y., X. Duan, Q. Wei, and C. M. Lieber, Directed assembly of one-dimensional nanostructures into functional networks, *Science* **291**, 630 (2001a).

Huang, Y., X. Duan, Y. Cui, L. J. Lauhon, K. H. Kim, and C. M. Lieber, Logic gates and computation from assembled nanowire building blocks, *Science* **294**, 1313 (2001b).

Iijima, S. Helical microtubules of graphitic carbon, *Nature* **354**, 56 (1991).

Iijima, S., Growth of carbon nanotubes, *Materials Science & Engineering B* **19**, 172 (1993).

Iijima, S., and T. Ichihashi, Single-shell carbon nanotubes of 1-nm diameter, *Nature* **363**, 603 (1993).

Javey, A., M. Shim, and H. Dai, Electrical properties and devices of large-diameter single-walled carbon nanotubes, *Appl. Phys. Lett.* **80**, 1064 (2002).

Journet, C., W. Maser, P. Bernier, A. Loiseau, M. de la Chapelle, S. Lefrant, P. Deniard, R. Lee, and J. Fischer, Large-scale production of single-walled carbon nanotubes by the electric-arc technique, *Nature* **388**, 756 (1997).

Kane, C. L., and E. J. Mele, Size, shape, and low energy electronic structure of carbon nanotubes, *Phys. Rev. Lett.* **78**, 1932 (1997).

Kane, C., L. Balents, and M. P. A. Fisher, Coulomb interactions and mesoscopic effects in carbon nanotubes, *Phys. Rev. Lett.* **79**, 5086 (1997).

Kim, P., L. Shi, A. Majumdar, and P. L. McEuen, Thermal transport measurements of individual multiwalled nanotubes, *Phys. Rev. Lett.* **87**, 215502 (2001).

Kong, J., and H. Dai, Full and modulated chemical gating of individual carbon nanotubes by organic amine compounds, *J. Phys. Chem. B* **105**, 2890 (2001).

Kong, J., H. T. Soh, A. Cassell, C. F. Quate, and H. Dai, Synthesis of single single-walled carbon nanotubes on patterned silicon wafers, *Nature* **395**, 878 (1998).

Kong, J., C. Zhou, E. Yenilmez, and H. Dai, Alkaline metal-doped n-type semiconducting nanotubes as quantum dots. *Appl. Phys. Lett.* **77**, 3977 (2000a).

Kong, J., N. R. Franklin, C. Zhou, M. G. Chapline, S. Peng, K. Cho, and H. Dai, Nanotube molecular wires as chemical sensors, *Science* **287**, 622 (2000b).

Kong, J., E. Yenilmez, T. W. Tombler, W. Kim, H. Dai, R. B. Laughlin, L. Liu, C. S. Jayanthi, and S. Y. Wu, Quantum interference and ballistic transmission in nanotube electron waveguides, *Phys. Rev. Lett.* **87**, 106801 (2001).

Kong, J., J. Cao, and H. Dai, Chemical profiling of single nanotubes: intramolecular p–n–p junctions and on-tube single-electron transistors, *Appl. Phys. Lett.* **80**, 73 (2002).

Kouwenhoven, L. R., C. M. Marcus, P. L. McEuen, S. Tarucha, R. Westervelt, and N. S. Wingreen, Electron transport in quantum dots, in *Mesoscopic Electron Transport* edited by L.L. Sohn, L. P. Kouwenhoven, and G. Schon Kluwer, Boston, MA (1997).

Krishnan, K. M., J. Kouvetakis, T. Sasaki, and N. Bartlett, Characterization of newly synthesized novel graphite films, in *Better Ceramics Through Chemistry III. Symposium*

edited by C. J. Brinker, D. E. Clark, and D. R. Ulrich, Material Research Society, Pittsburgh, PA, p. 527 (1988).

Landauer, R., *IBM J. Res. Dev.* **1**, 223 (1958).

Lee, R. S., J. Gavillet, M. L. de la Chapelle, A. Loiseau, J. L. Cochon, D. Pigache, J. Thibault, and F. Willaime, Catalyst-free synthesis of boron nitride single-wall nanotubes with a preferred zig-zag configuration, *Phys. Rev. B (Condens. Matter Mater. Phys.)* **64**, 121405 (2001).

Lefebvre, J., M. Radosavljevic, and A. T. Johnson, Fabrication of nanometer size gaps in a metallic wire, *Appl. Phys. Lett.* **76**, 3828 (2000).

Leonard, J., and F. Tersoff, Novel length scales in nanotube devices, *Phys. Rev. Lett.* **83**, 5174 (1999).

Li, J., C. Papadopoulos, and J. Xu, Nanoelectronics: growing Y-junction carbon nanotubes, *Nature* **402**, 253 (1999).

Li, W. Z., J. G. Wen, and Z. F. Ren, Straight carbon nanotube Y junctions, *Appl. Phys. Lett.* **79**, 1879 (2001).

Li, Y., W. Kim, Y. Zhang, M. Rolandi, D. Wang, and H. Dai, Growth of single-walled carbon nanotubes from discrete catalytic nanoparticles of various sizes, *J. Phys. Chem. B* **105**, 11424 (2001).

Liang, W., M. Bockrath, D. Bozovic, J. H. Hafner, M. Tinkham, and H. Park, Fabry–Perot interference in a nanotube electron waveguide, *Nature* **411**, 665 (2001).

Liu, J., A. G. Rinzler, H. Dai, J. H. Hafner, R. K. Bradley, P. J. Boul, A. Lu, T. Iverson, K. Shelimov, C. B. Huffman, F. Rodriguez-Macias, Y.-S. Shon, T. R. Lee, D. T. Colbert, and R. E. Smalley, Fullerene pipes, *Science* **280**, 1253 (1998).

Liu, J., M. J. Casavant, M. Cox, D. A. Walters, P. Boul, L. Wei, A. J. Rimberg, K. A. Smith, D. T. Colbert, and R. E. Smalley, Controlled deposition of individual single-walled carbon nanotubes on chemically functionalized templates, *Chem. Phys. Lett.* **303**, 125 (1999).

Loiseau, A., F. Willaime, N. Demoncy, G. Hug, and H. Pascard, Boron nitride nanotubes with reduced numbers of layers synthesized by arc discharge, *Phys. Rev. Lett.* **76**, 4737 (1996).

Louie, S. G., Electronic properties, junctions, and defects of carbon nanotubes, in *Topics in Applied Physics* edited by M. S. Dresselhaus, G. Dresselhaus, and P. Avouris, Vol. 80, Springer, Berlin, p. 113 (2001).

Martel, R., T. Schmidt, H. R. Shea, T. Hertel, and P. Avouris, Single- and multi-wall carbon nanotube field-effect transistors, *Appl. Phys. Lett.* **73**, 2447 (1998).

Martel, R., V. Derycke, C. Lavoie, J. Appenzeller, K. K. Chan, J. Tersoff, and P. Avouris, Ambipolar electrical transport in semiconducting single-wall carbon nanotubes, *Phys. Rev. Lett.* **87**, 256805 (2001).

Matsumoto, K., M. Ishii, K. Segawa, Y. Oka, B. J. Vartanian, and J. S. Harris, Room temperature operation of a single electron transistor made by the scanning tunneling microscope nanooxidation process for the TiO_x/Ti system, *Appl. Phys. Lett.* **68**, 34 (1996).

McEuen, P. L., Single-wall carbon nanotubes, *Phys. World* (2000).

McEuen, P. L., M. Bockrath, D. H. Cobden, Y.-G. Yoon, and S. G. Louie, Disorder, pseudospins, and backscattering in carbon nanotubes, *Phys. Rev. Lett.* **83**, 5098 (1999).

Menon, M., and D. Srivastava, Carbon nanotube "T junctions": nanoscale metal–semiconductor–metal contact devices, *Phys. Rev. Lett.* **79**, 4453 (1997).

Mickelson, E. T., C. B. Huffman, A. G. Rinzler, R. E. Smalley, R. H. Hauge, and J. L. Margrave, Fluorination of single-wall carbon nanotubes, *Chem. Phys. Lett.* **296**, 188 (1998).

Mintmire, J. W., and C. T. White, Universal density of states for carbon nanotubes, *Phys. Rev. Lett.* **81**, 2506 (1998).

Mintmire, J. W., B. I. Dunlap, and C. T. White, Are fullerene tubules metallic? *Phys. Rev. Lett.* **68**, 631 (1992).

Miyamoto, Y., A. Rubio, M. L. Cohen, and S. G. Louie, Chiral tubules of hexagonal BC_2N, *Phys. Rev. B (Condens. Matter)* **50**, 4976 (1994a).

Miyamoto, Y., A. Rubio, S. G. Louie, and M. L. Cohen, Electronic properties of tubule forms of hexagonal BC_3, *Phys. Rev. B (Condens. Matter)* **50**, 18360 (1994b).

Miyamoto, Y., S. G. Louie, and M. L. Cohen, Chiral conductivities of nanotubes, *Phys. Rev. Lett.* **76**, 2121 (1996).

Miyamoto, Y., A. Rubio, S. G. Louie, and M. L. Cohen, Self-inductance of chiral conducting nanotubes, *Phys. Rev. B (Condens. Matter)* **60**, 13885 (1999).

Morales, A. M., and C. M. Lieber, A laser ablation method for the synthesis of crystalline semiconductor nanowires, *Science* **279**, 208 (1998).

Nakanishi, T., and T. Ando, Numerical study of impurity scattering in carbon nanotubes, *J. Phys. Soc. Jpn.* **68**, 561 (1999).

Niyogi, S., H. Hu, M. A. Hamon, P. Bhowmik, B. Zhao, S. M. Rozenzhak, J. Chen, M. E. Itkis, M. S. Meier, and R. C. Haddon, Chromatographic purification of soluble single-walled carbon nanotubes (s-SWNTs), *J. Am. Chem. Soc.* **123**, 733 (2001).

Nygard, J., D. H. Cobden, M. Bockrath, P. L. McEuen, and P. E. Lindelof, Electrical transport measurements on single-walled carbon nanotubes, *Appl. Phys. A (Mater. Sci. Process.)* **A69**, 297 (1999).

Nygard, J., D. H. Cobden, and P. E. Lindelof, Kondo physics in carbon nanotubes, *Nature* **408**, 342 (2000).

Odintsov, A. A. Schottky barriers in carbon nanotube heterojunctions, *Phys. Rev. Lett.* **85**, 150 (2000).

Odom, T. W., H. Jin-Lin, P. Kim, and C. M. Lieber, Atomic structure and electronic properties of single-walled carbon nanotubes, *Nature* **391**, 62 (1998).

Park, H., J. Park, A. K. L. Lim, E. H. Anderson, A. P. Alivisatos, and P. L. McEuen, Nanomechanical oscillations in a single-C_{60} transistor, *Nature* **407**, 57 (2000).

Park, J., and P. L. McEuen, Formation of a p-type quantum dot at the end of an n-type carbon nanotube, *Appl. Phys. Lett.* **79**, 1363 (2001).

Pashkin, Y. A., Y. Nakamura, and J. S. Tsai, Room-temperature Al single-electron transistor made by electron-beam lithography, *Appl. Phys. Lett.* **76**, 2256 (2000).

Peierls, R. E. *Quantum Theory of Solids*, Oxford University Press, New York (1955).

Poncharal, P., Z. L. Wang, D. Ugarte, and W. A. De Heer, Electrostatic deflections and electromechanical resonances of carbon nanotubes, *Science* **283**, 1513 (1999).

Postma, H. W. C., M. de Jonge, and C. Dekker, Electrical transport through carbon nanotube junctions created by mechanical manipulation, *Phys. Rev. B (Condens. Matter)* **62**, R10653 (2000).

Postma, H. W. C., T. Teepen, Y. Zhen, M. Grifoni, and G. Dekker, Carbon nanotube single-electron transistors at room temperature, *Science* **293**, 76 (2001).

Rao, A. M., E. Richter, S. Bandow, B. Chase, P. C. Eklund, K. A. Williams, S. Fang, K. R. Subbaswamy, M. Menon, A. Thess, R. E. Smalley, G. Dresselhaus, and M. S. Dresselhaus, Diameter-selective Raman scattering from vibrational modes in carbon nanotubes, *Science* **275**, 187 (1997).

Remskar, M., A. Mrzel, Z. Skraba, A. Jesih, M. Ceh, J. Demsar, P. Stadelmann, F. Levy, and D. Mihailovic, Self-assembly of subnanometer-diameter single-wall MoS_2 nanotubes, *Science* **292**, 479 (2001).

Reulet, B., A. Y. Kasumov, M. Kociak, R. Deblock, I. I. Khodos, Y. B. Gorbatov, V. T. Volkov, C. Journet, and H. Bouchiat, Bolometric detection of mechanical bending waves in suspended carbon nanotubes, *Condens. Matter Arch.* (xxx.lanl.gov) (1999).

Riggs, J. E., Z. Guo, D. L. Carroll, and Y.-P. Sun, Strong luminescence of solubilized carbon nanotubes, *J. Am. Chem. So.* **122**, 5879 (2000).

Rinzler, A. G., J. Liu, H. Dai, P. Nikolaev, C. B. Huffman, F. J. Rodriguez-Macias, P. J. Boul, A. H. Lu, D. Heymann, D. T. Colbert, R. S. Lee, J. E. Fischer, A. M. Rao, and R. E. Smalley, Large-scale purification of single-wall carbon nanotubes: process, product, and characterization, *Appl. Phys. A (Mater. Sci. Process.)* **67**, 29 (1998).

Rubio, A., J. L. Corkill, and M. L. Cohen, Theory of graphitic boron nitride nanotubes, *Phys. Rev. B (Condens. Matter)* **49**, 5081 (1994).

Rueckes, T., K. Kim, E. Joselevich, G. Y. Tseng, C. L. Cheung, and C. M. Lieber, Carbon nanotube-based nonvolatile random access memory for molecular computing, *Science* **289**, 94 (2000).

Saito, R., M. Fujita, G. Dresselhaus, and M. S. Dresselhaus, Electronic structure of graphene tubules based on C_{60}, *Phys. Rev. B (Condens. Matter)* **46**, 1804 (1992a).

Saito, R., M. Fujita, G. Dresselhaus, and M. S. Dresselhaus, Electronic structure of chiral graphene tubules, *Appl. Phys. Lett.* **60**, 2204 (1992b).

Saito, R., G. Dresselhaus, and M. S. Dresselhaus, Tunneling conductance of connected carbon nanotubes, *Phys. Rev. B (Condens. Matter)* **53**, 2044 (1966).

Satishkumar, B. C., P. J. Thomas, A. Govindaraj, and C. N. R. Rao, Y-junction carbon nanotubes, *Appl. Phys. Lett.* **77**, 2530 (2000).

Schlittler, R. R., J. W. Seo, J. K. Gimzewski, C. Durkan, M. S. M. Saifullah, and M. E. Welland, Single crystals of single-walled carbon nanotubes formed by self-assembly, *Science* **292**, 1136 (2001).

Schonenberger, C., and L. Forro, Multiwall carbon nanotubes, *Phys. World* (2000).

Schonenberger, C., A. Bachtold, C. Strunk, J. P. Salvetat, and L. Forro, Interference and interaction in multi-wall carbon nanotubes, *Appl. Phys. A (Mater. Sci. Process.)* **A69**, 283 (1999).

Sedeki, A., L. G. Caron, and C. Bourbonnais, Electron–phonon coupling and Peierls transition in metallic carbon nanotubes, *Phys. Rev. B (Condens. Matter)* **62**, 6975 (2000).

Su, W. P., J. R. Schrieffer, and A. J. Heeger, Soliton excitations in polyacetylene, *Phys. Rev. B (Condens. Matter Mater. Phys.)* **22**, 2099 (1980).

Suenaga, K., C. Carbon, N. Demoncy, A. Loiseau, H. Pascard, and F. Williame, Synthesis of nanoparticles and nanotubes with well-separated layers of boron nitride and carbon, *Science* **278**, 653 (1997).

Tans, S. J., M. H. Devoret, H. Dai, A. Thess, R. E. Smalley, L. J. Georliga, and C. Dekker, Individual single-wall carbon nanotubes as quantum wires, *Nature* **386**, 474 (1997).

Tans, S. J., M. H. Devoret, R. J. A. Groeneveld, and C. Dekker, Electron–electron correlations in carbon nanotubes, *Nature* **394**, 761 (1998a).

Tans, S. J., R. M. Verschueren, and C. Dekker, Room temperature transistor based on a single carbon nanotube, *Nature* **393**, 49 (1998b).

Tenne, R., and A. K. Zettl, Nanotubes from inorganic materials, in *Topics in Applied Physics*, edited by M. S. Dresselhaus, G. Dresselhaus, and P. Avouris, Vol. 80, Springer, Berlin, p. 81 (2001).

Thess, A., R. Lee, P. Nikolaev, H. Dai, P. Petit, J. Robert, C. Xu, Y. H. Lee, S. G. Kim, A. G. Rinzler, D. T. Colbert, G. E. Scuseria, D. Tomanek, J. E. Fischer, and R. E. Smalley, Crystalline ropes of metallic carbon nanotubes, *Science* **273**, 483 (1996).

Ting, J.-M., and C.-C. Chang, Multijunction carbon nanotube network, *Appl. Phys. Lett.* **80**, 324 (2002).

Treacy, M. M. J., T. W. Ebbesen, and J. M. Gibson, Exceptionally high Young's modulus observed for individual carbon nanotubes, *Nature* **381**, 678 (1996).

Trentler, T. J., K. M. Hickman, S. C. Goel, A. M. Viano, P. C. Gibbons, and W. E. Buhro, Solution–liquid–solid growth of crystalline III–V semiconductors: an analogy to vapor–liquid–solid growth, *Science* **270**, 1791 (1995).

Venkataraman, L., and C. M. Lieber, Molybdenum selenide molecular wires as one-dimensional conductors, *Phys. Rev. Lett.* **83**, 5334 (1999).

Wagner, R. S, in *Whisker Technology*, edited by A. P. Levitt Wiley-Interscience, New York, p. 47 (1970).

Wagner, R. S., and W. C. Ellis, *Appl. Phys. Lett.* **4**, 89 (1964).

Wei, B. Q., R. Vajtai, and P. M. Ajayan, Reliability and current carrying capacity of carbon nanotubes, *Appl. Phys. Lett.* **79**, 1172 (2001).

Weiqiang, H., Y. Bando, K. Kurashima, and T. Sato, Synthesis of boron nitride nanotubes from carbon nanotubes by a substitution reaction, *Appl. Phys. Lett.* **73**, 3085 (1998).

Weng-Sieh, Z., K. Cherrey, N. G. Chopra, X. Blase, Y. Miyamato, A. Rubio, M. L. Cohen, S. G. Louie, A. Zettl, and R. Gronsky, Synthesis of $B_xC_yN_z$ nanotubules, *Phys. Rev. B (Condens. Matter)* **51**, 11229 (1995).

Westwater, J., D. P. Gosain, S. Tomiya, S. Usui, and H. Ruda, Growth of silicon nanowires via gold/silane vapor–liquid–solid reaction, *J. Vac. Sci. Technol. B (Microelectron. Nanometer Struct.)* **15**, 554 (1997).

White, C. T., and T. N. Tudorov, Carbon nanotubes as long ballistic conductors, *Nature* **393**, 240 (1998).

Wildoer, J. W. G., L. C. Venema, A. G. Rinzler, R. E. Smalley, and C. Dekker, Electronic structure of atomically resolved carbon nanotubes, *Nature* **391**, 59 (1998).

Wong, E. W., P. E. Sheehan, and C. M. Lieber, Nanobeam mechanics: elasticity, strength and toughness of nanorods and nanotubes, *Science* **277**, 1971 (1997).

Woodside, M. T., C. Vale, P. L. McEuen, C. Kadow, K. D. Maranowski, and A. C. Gossard, Imaging interedge-state scattering centers in the quantum Hall regime, *Phys. Rev. B (Condens. Matter Mater. Phys.)* **64**, 041310 (2001).

Yakobson, B. I., and P. Avouris, Mechanical properties of carbon nanotubes, in *Topics in Applied Physics*, edited by M. S. Dresselhaus, G. Dresselhaus, and P. Avouris, Vol. 80, Springer, Berlin, p. 287 (2001).

Yao, Z., C. L. Kane, and C. Dekker, High-field electrical transport in single-wall carbon nanotubes, *Phys. Rev. Lett.* **84**, 2941 (2000).

Yao, Z., C. Dekker, and P. Avouris, Electrical transport through single-wall carbon nanotubes, in *Topics in Applied Physics*, edited by M. S. Dresselhaus, G. Dresselhaus, and P. Avouris, Vol. 80, Springer, Berlin, p. 147 (2001).

Yazawa, M., M. Koguchi, A. Muto, M. Ozawa, and K. Hiruma, Effect of one monolayer of surface gold atoms on the epitaxial growth of InAs nanowhiskers, *Appl. Phys. Lett.* **61**, 2051 (1992).

Yu, D. P., X. S. Sun, C. S. Lee, I. Bello, S. T. Lee, H. D. Gu, K. M. Leung, G. W. Zhou, Z. F. Dong, and Z. Zhang, Synthesis of boron nitride nanotubes by means of excimer laser ablation at high temperature, *Appl. Phys. Lett.* **72**, 1966 (1998).

Zhang, Y. F., Y. H. Tang, N. Wang, D. P. Yu, C. S. Lee, I. Bello, and S. T. Lee, Silicon nanowires prepared by laser ablation at high temperature, *Appl. Phys. Lett.* **72**, 1835 (1998).

Zhou, C., J. Kong, E. Yenilmez, and H. Dai, Modulated chemical doping of individual carbon nanotubes, *Science* **290**, 1552 (2000).

Zhuang, L., L. Guo, and S. Y. Chou, Silicon single-electron quantum-dot transistor switch operating at room temperature, *Appl. Phys. Lett.* **72**, 1205 (1998).

Zunger, A., A. Katzir, and A. Halperin, Optical properties of hexagonal boron nitride, *Phys. Rev. B (Solid State)* **13**, 5560 (1976).